# Common-garden study of introgression at loci associated with traits adaptive to coastal environment from Quercus dentata into Q. mongolica var. crispula

Teruyoshi Nagamitsu[1], Kentaro Uchiyama[1], Ayako Izuno[1], and Hajime Shimizu[2]

[1]Forest Research and Management Organisation
[2]Hokkaido Research Organisation Forest Research Department

August 19, 2023

**Abstract**

Adaptive introgression has been proposed in oaks (genus Quercus). In northern Japan, Q. mongolica var. crispula (Qc) is common in inland habitats, and Q. dentata (Qd) occurs in coastal habitats. At the northern distributional limit of Qd, Q. × angustilepidota (Qa), a hybrid taxon between Qc and Qd, occurs in coastal habitats. The three taxa, Qc, Qa, and Qd, were transplanted to inland and coastal common gardens (sites). Genotypes at 27495 loci, phenotypes of eight traits of leaves and shoots, and 30-year-old tree size were measured for 224 individuals in both sites. Genotypic variation revealed a hybrid zone between Qc and Qd, including both northern-edge Qd admixed with Qc and coastal Qa backcrossed to Qc. Phenotypes of Qa trees were intermediate between those of Qc and Qd trees. Size of Qa and Qd trees was smaller than that of Qc trees in the inland site but was larger in the coastal site, suggesting adaptation of Qa and Qd to coastal environment. Local ancestry was estimated from phased genotypes of admixed trees using reference genotypes of 47 Qc and 25 Qd trees, indicating heterogeneous ancestry along chromosomes. Association mapping of genotypes and admixture mapping of ancestry suggested that some loci potentially associated with four traits were related to stress response and were located at introgressed genomic regions. Further studies are necessary to show the genetic basis of adaptive introgression resulting in Qd-like phenotypes of Qa in coastal habitats.

**Title**

Common-garden study of introgression at loci associated with traits adaptive to coastal environment from *Quercus dentata* into *Q. mongolica* var. *crispula*

**Authors**

Teruyoshi Nagamitsu,[1] Kentaro Uchiyama,[1] Ayako Izumo,[1] and Hajime Shimizu[2]

**Affiliations**

[1] Department of Forest Molecular Genetics and Biotechnology, Forestry and Forest Products Research Institute, Forest Research and Management Organization, Tsukuba 305-8687, Japan

[2] Donan Station, Forestry Research Department, Hokkaido Research Organization, Hakodate 041-0801, Japan

**Author for Correspondence**

Teruyoshi Nagamitsu orcid.org/0000-0003-3366-7197

nagamit@affrc.go.jp

+81-29-829-8264

**Contacts of co-authors**

Kentaro Uchiyama orcid.org/0000-0003-4083-3034

kruchiyama@affrc.go.jp

Ayako Izumo orcid.org/0000-0002-9339-2845

izuno@ffpri.affrc.go.jp

Hajime Shimizu

shimizu-hajime@hro.or.jp

**Abstract**

Adaptive introgression has been proposed in oaks (genus *Quercus* ). In northern Japan, *Q. mongolica* var. *crispula* ( *Qc* ) is common in inland habitats, and *Q. dentata* ( *Qd* ) occurs in coastal habitats. At the northern distributional limit of *Qd* ,*Q.* × *angustilepidota* ( *Qa* ), a hybrid taxon between *Qc* and *Qd* , occurs in coastal habitats. The three taxa, *Qc* , *Qa* , and *Qd* , were transplanted to inland and coastal common gardens (sites). Genotypes at 27495 loci, phenotypes of eight traits of leaves and shoots, and 30-year-old tree size were measured for 224 individuals in both sites. Genotypic variation revealed a hybrid zone between *Qc* and *Qd* , including both northern-edge *Qd* admixed with *Qc* and coastal *Qa* backcrossed to *Qc* . Phenotypes of *Qa* trees were intermediate between those of *Qc* and *Qd* trees. Size of *Qa* and *Qd* trees was smaller than that of *Qc* trees in the inland site but was larger in the coastal site, suggesting adaptation of *Qa* and *Qd* to coastal environment. Local ancestry was estimated from phased genotypes of admixed trees using reference genotypes of 47 *Qc* and 25 *Qd* trees, indicating heterogeneous ancestry along chromosomes. Association mapping of genotypes and admixture mapping of ancestry suggested that some loci potentially associated with four traits were related to stress response and were located at introgressed genomic regions. Further studies are necessary to show the genetic basis of adaptive introgression resulting in *Qd* -like phenotypes of *Qa* in coastal habitats.

**Keywords**

adaptive introgression, genome-wide association study, hybridization, local ancestry, phenotypic plasticity

## 1 | Introduction

Introgression is the transfer of alleles from one taxon (donor) into genomes of another taxon (recipient) through hybridization, recombination, and backcrossing (Anderson 1953; Barton and Hewitt 1985). Generally, alleles introgressed from the donor taxon can be deleterious, because of conflicting interactions in the genomes and unfavorable phenotypes in the environment of the recipient taxon (Burke and Arnold 2001; Goulet et al. 2017). Thus, introgressed alleles will be purged from the recipient genomes, and the genetic integrity of each taxon can be maintained (Rieseberg and Carney 1998). However, in specific environment, where the donor-like phenotypes are more adaptive than the recipient phenotypes, introgressed alleles can be selected and fixed in the recipient genomes (Anderson and Stebbins 1954; Suarez-Gonzalez et al. 2018c). Such environment-dependent adaptive introgression has been found in some plants, resulting in the expansion to novel habitats and the creation of different ecotypes in the recipient taxa (Martin et al. 2006; Rieseberg et al. 2007; Whitney et al. 2010; Arnold et al. 2016). Adaptive introgression tends to occur at distributional range margins of either taxon, where hybridization with the other taxon is frequent due to reduced opportunity of mating within marginal populations, and introgressed populations of the recipient taxa can colonize habitats suitable for the donor taxa (Chhatre et al. 2018; Ma et al. 2019; Menon et al. 2021; Rendón-Anaya et al. 2021). This process is thought to contribute colonization and range shift of forest trees during past climate change and offer an option of forest management under future climate change (Petit et al. 2004; Hamilton and Miller 2016).

Oaks (genus *Quercus* , Fagaceae) are temperate forest trees in the northern hemisphere and are often interfertile among species (Denk et al. 2017). Introgression between oak taxa has long been proposed (Stebbins

et al. 1947; Sork et al. 2016), and their genomes are regarded as phylogenetic mosaics of different origins (Kim et al. 2018; Hipp et al. 2020). Oaks inhabiting heterogeneous environments usually have different phenotypic and genetic variations (Ortego et al. 2014; Riordan et al. 2016; Cavender-Bares 2019) and often exhibit local adaptation to indigenous environments (Sork 2018; Leroy et al. 2020). In northern Japan, there are two species of white oaks (section *Quercus* ),*Q. mongolica* Fischer ex Ledebour var. *crispula* (Blume) H. Ohashi (*Qc* ) is common in inland habitats, and *Q. dentata*Thunberg ex Murray (*Qd* ) occurs in coastal habitats (Matsumoto et al. 2009). In northern Hokkaido, *Qd* trees are rare because this area is the northern distributional limit of *Qd* , whereas*Qc* trees are abundant because *Qc* is distributed to more northern area, Sakhalin. In the northernmost area of Hokkaido, a coastal*Qc* ecotype with unique traits, which are similar to *Qd*phenotypes and tolerant to coastal stress, occurs in coastal forests (Nagamitsu et al. 2019). Some taxonomists regarded this coastal*Qc* ecotype as a hybrid taxon *Q.* × *angustilepidota*Nakai (*Qa* ) between *Qc* and *Qd* (Ohba 2006; Aizawa et al. 2021). Multi-locus nuclear microsatellite genotypes supported this hybrid origin (Nagamitsu et al. 2019), and genome-wide single nucleotide polymorphism (SNP) genotypes demonstrated environment-dependent introgression from *Qd* to *Qc* , resulting in *Qa* that included hybrids after the first generation of backcross to *Qc*(Nagamitsu et al. 2020). Thus, introgression of *Qd* alleles to*Qc* genomes at loci associated with traits adaptive to coastal environment is expected but has not been confirmed yet.

Oak trees in coastal habitats suffer from various stress, such as wind, salinity, drought, heat, substrate instability, and nutrient scarcity (Hesp 1991). For example, strong wind and salt spray in winter cause the mortality of buds in the upper parts of shoots, resulting in frequent dieback of shoots, slow elongation of stems, and low canopy height of coastal oak forests (Asai et al. 1986). These stresses are likely to cause natural selection in leaf and shoot traits, leading to local adaptation (Ramírez-Valiente et al. 2010; Ciccarelli and Bona 2022). Common-garden experiment using inland and coastal test sites is effective to show local adaptation in *Qc* and *Qd* . Relatively higher performance of *Qa* trees with *Qd* -like phenotypes of leaf and shoot traits in coastal sites than in inland sites will indicate the adaptation of these traits to coastal habitats. Difference in phenotypes among admixed trees between inland and coastal habitats depends not only on genetic and environmental variations but also on their interaction, namely phenotypic plasticity (Ramírez-Valiente et al. 2010). Common-garden experiment is useful to elucidate phenotypic plasticity and to discriminate genetic variation from environmental variation in phenotypes.

Phenotypes of admixed recombinants in common gardens enable us to detect loci associated with focal traits (Rieseberg and Buerkle 2002). This approach is referred to as admixture mapping and is useful in long-lived and large-sized organisms, for which pedigrees from artificial crosses are difficult to obtain (Buerkle and Lexer 2008). In poplar, one of the forest trees with rich genomic information, admixture mapping was applied to various traits (Suarez-Gonzalez et al. 2018a; Bresadola et al. 2019). Admixture mapping requires the inference of locus-specific (local) ancestry, the number of alleles that originate from either ancestral population involved in the admixture at individual loci (Lindtke et al. 2013). Local ancestry usually deviates from genome-wide ancestry of individuals, indicating the excess or deficit of admixture at individual loci (Buerkle and Lexer 2008). A genome-wide pattern of introgression is often illustrated using various approaches (Martin and Van Belleghem 2017), for example, the Paterson's $D$ statistics from the ABBA-BABA test that discriminates introgression from incomplete lineage sorting (Martin et al. 2015). These approaches require a sufficient number of genome-wide loci, which can be obtained from sequences of reduced genomic libraries mapped to a whole-genome reference sequence that has been available in white oaks (Plomion et al. 2018; Sork et al. 2022). Recently, reference sequences of *Q. mongolica* var. *mongolica* and *Qd* also has been published (Ai et al. 2022; Wang et al. 2023). Using genotypes, phenotypes, and performance of trees admixed between *Qc* and *Qd* in common gardens, we can verify adaptive introgression of *Qd* alleles at loci associated with adaptive traits into *Qc* genome.

In this study, we tried to obtain evidence for the adaptive introgression using inland and coastal common gardens (sites), where seedlings of the focal white oak taxa, *Qc* , *Qa* , and*Qd* , were planted from various provenances in Hokkaido and had now reached about 30 years old. First, we examined their genetic variation using genome-wide SNP genotypes to estimate genomic compositions of hybrids and genome-wide patterns

of introgression. Next, we measured phenotypes of leaf and shoot traits and performance of trees in each site to demonstrate adaptation of *Qd* -like phenotypes of these traits to coastal environment. Finally, we searched for loci, at which SNP genotypes and local ancestry were associated with those traits. We expected that these trait-associated loci were located at introgressed genomic regions and were close to genes involved in adaptation to coastal environment.

## 2 | Materials and methods

### 2.1 | Common gardens

Two common gardens were established in an inland site (44.7@N, 142.1@E, 20 m elevation) and a coastal site (45.3@N, 141.6@E, 5 m elevation) in northern Hokkaido (Figure S1 in Supporting Information). In each site, the three taxa, *Quercus mongolica* var. *crispula*( *Qc* ), *Q. dentata* ( *Qd* ), and their hybrids, *Q.*× *angustilepidota* ( *Qa* ), were transplanted from natural forests in 32 provenances in Hokkaido (Figure 1, Table S1). Acorns (seeds) of several maternal trees were collected from a forest stand in each provenance, and their seedlings were reared in a nursery in the Dohoku Station of the Forestry Research Institute of the Hokkaido Research Organization. In the inland site located in the Dohoku Station, seedlings were planted at 1.4 m intervals along plantation rows spaced 2.8 m apart in three blocks in 1992–1993, and half of trees in two blocks and a few trees in one block were thinned in 2006, when tree crowns became crowded (Figure S2). In the coastal site on sand dunes at 500 m distance from the seashore, seedlings were planted at 0.8 m intervals along plantation rows spaced 2.8 m apart in two blocks in 1986, and trees were not thinned because tree crowns had been sparse (Figure S3).

We observed living trees in both sites and identified the taxa of trees in 2017–2019 (Figures S2, S3). Because taxonomic identification of*Qc* and *Qd* is ambiguous due to intermediate phenotypes (Ohba 2006; Aizawa et al. 2021), we classified the taxa using the following criteria based on hairs on shoots according to our previous studies (Nagamitsu et al. 2019; Nagamitsu et al. 2020). Trees with pubescent one-year-old shoots with trichomes (stellate hairs) were identified as *Qd* . Among trees with glabrous one-year-old shoots, trees from provenances in coastal habitats, sand dunes and coastal cliffs, were identified as *Qa* , which was recognized as the coastal ecotype of *Qc* in the previous studies (Nagamitsu et al. 2019; Nagamitsu et al. 2020), and trees from provenances in inland habitats, hills and mountains, were identified as *Qc* (Table S1). In addition to living trees, we observed dead trees that had died recently. We were not able to record individuals that had died when they were saplings. We confirmed the provenances of living and dead trees based on plantation records of the common gardens.

The following measurement and collection were conducted in both sites in 2017–2019. We measured the girth (cm) of every stem of each living tree to evaluate tree size. The girth at the breast height in the inland site and that at the ground level in the coastal site were measured, because trees in the coastal site were crooked and branching near the ground due to strong wind. The locations of living and dead trees and the girths of living trees of *Qc* , *Qa* , and *Qd* were recorded in both sites (Figures S2, S3). We collected some branches of trees sampled from living trees in July to obtain DNA and to measure phenotypes. Some flesh leaves on current-year shoots were stored at –20@C, and DNA was extracted from leaf tissues using DNeasy Plant Mini Kit (Qiagen, Hilden, Germany). Three leaves on current-year shoots and three one-year-old shoots selected from collected branches of each sampled tree were dried and preserved for morphological measurement.

### 2.2 | Genotyping

A double-digest restriction-site-associated DNA (ddRAD) library was prepared using a modified protocol of the standard method (Peterson et al. 2012) described in our previous study (Nagamitsu et al. 2020). Extracted DNA was digested with *Pst* I and *Sau* 3AI restriction enzymes, ligated with Y-shaped adaptors, and amplified by polymerase chain reaction (PCR) with the KAPA HiFi polymerase (Kapa Biosystems, Woburn, MA, USA). After PCR amplification with adapter-specific primer pairs (Access Array Barcode Library for Illumina, Fluidigm, South San Francisco, CA, USA), an equal amount of DNA from each tree was mixed and size-selected with the BluePippin agarose gel (Sage Science, Beverly, MA, USA). Approximately 450-bp library fragments were retrieved. The library quality was checked using a 2100 Bioanalyzer with a

high sensitivity DNA chip (Agilent Technologies, Waldbronn, Germany). The ddRAD library was sequenced using Illumina MiSeq and HiSeq to generate paired-end reads with a 150-bp length.

Obtained reads were mapped to the reference sequences consisting of 12 pseudomolecules (chromosomes) of the *Q. robur* genome assembly PM1N (Plomion et al. 2018). Although some reference sequences of white oak species including *Q. mongolica* var. *mongolica* and *Qd* are available (Sork et al. 2022; Ai et al. 2022; Wang et al. 2023), we selected PM1N because *Q. robur* is a species closely-related to the common ancestor of *Qc* and *Qd* . The read mapping and variant calling were conducted using dDocent 2.7.8 (Puritz et al. 2014). The subsequent filtering procedures in detail are explained in our previous study (Nagamitsu et al. 2020). From the variant loci with various types of polymorphism, we selected loci that were biallelic without indels and polymorphic with high sequencing quality, $< 5\%$ missing genotypes, and $> 5\%$ minor allele frequency, using VCFtools 0.1.14 (Danecek et al. 2011). We removed loci mapped to the regions of transposable elements determined in *Q. robur* (Plomion et al. 2018). In addition, we removed loci that extremely deviated from the Hardy–Weinberg equilibrium ($P< 0.01$) probably due to null alleles within a population of each taxon, *Qc* , *Qa* , or *Qd* , using VCFtools.

### 2.3 | Genomic composition

To summarize genetic structure of sampled trees in the inland and coastal sites and to obtain allele frequencies in ancestral populations that represent *Qc* and *Qd* , we conducted Bayesian clustering for SNP genotypes at ddRAD loci using Admixture 1.3 (Alexander and Lange 2011). The log-likelihood was obtained, when the number ($K$ ) of ancestral populations (clusters) was 1, 2, or 3. Allele frequencies at ddRAD loci in each cluster ($P$ ) and ancestry proportions of each cluster in individual trees ($Q$ ) were estimated for each $K$ . Genetic differentiation between clusters (pairwise $F_{ST}$) was also estimated. We regarded two clusters ($K = 2$) as ancestral populations that represented *Qc* and *Qd* and estimated allele frequencies $P$ for the two clusters.

To describe genomic compositions of sampled trees in both sites, we estimated the proportion of alleles derived from *Qd* ancestral population ($S$ ) and the proportion of heterozygous loci with both alleles derived from *Qc* and *Qd* ancestral populations ($H$ ) using the package HIest 2.0 (Fitzpatrick 2012) in R 3.3.2 (R_Core_Team 2019). We regarded allele frequencies $P$ for the two clusters obtained from the Bayesian clustering as $P_1$ and $P_2$ allele frequencies of ancestral populations of *Qc* and *Qd* , respectively, and estimated $S$ (*Qd* ancestry) and $H$ (inter-ancestry heterozygosity) of individual trees using the function HIest with the options, method = SANN, iterations = 10000.

### 2.4 | Phenotyping

We measured eight morphological traits of leaves and shoots, which were thought to be distinctive between *Qc* and *Qd* and associated with the tolerance to coastal stress (Nagamitsu et al. 2019). Measurements for three leaves and three shoots of branches collected from each tree were averaged and regarded as a phenotypic value of each tree.

To describe leaf shape, three traits were recorded: relative leaf width, lateral vein interval, and tooth angle (Figure S4). Among the three traits, the two latter traits are important to identify *Qc* and *Qd* taxa (Ohba 2006; Aizawa et al. 2021). The length between the apex and base of each leaf and the width at the widest part of the leaf (mm) were measured, and the number of lateral veins were counted. Relative leaf width was calculated from (leaf width)/(leaf length), and lateral vein interval (mm) was calculated from (leaf length)/(number of lateral veins + 1). Tooth angle (@) was measured on a serration at the central part of each leaf.

The density and size of stellate hairs on leaves vary between *Qc* and *Qd* (Ishida et al. 2003) and may have ecological and physiological functions (Bickford 2016). Stellate hairs on the lower surface of each leaf were observed in a circular leaf area with a 3.1 mm diameter between lateral veins using a stereo microscope (Figure S4). The number of stellate hairs in each area were counted, and the density ($mm^{-2}$) was obtained. As the size of stellate hairs, the length of a radial filament (mm) of a typical stellate hair was measured

(Figure S4).

Leaf mass per area (LMA) and shoot diameter may be related with adaptation to intense light, severe drought, and strong wind in coastal habitats (Sancho-Knapik et al. 2021). A leaf disc with a 9 mm diameter was collected from the central part of each leaf (Figure S4), and the dry weight (mg) of each disc was measured after dehydration at 60@C for 48 h to calculate LMA (mg $mm^{-2}$). Shoot diameter (mm) was measured at the upper part of shoots. Salt spray and harsh wind in winter cause the mortality of buds, particularly those in the upper part of shoots (Asai et al. 1986). Bud production in the lower part of shoots is likely to convey the tolerance to coastal stress, because this bud production can compensate for high bud mortality in the upper part of shoots. Thus, the number of axillary buds at bud-scale scars located in the lowest part of shoots was recorded (Figure S4).

### 2.5 | Phenotypic variation

To summarize phenotypic variation of sampled trees in the inland and coastal sites, we performed principal component analyses (PCA) using the function prcomp in R 3.3.2. Among the eight traits, the frequency distributions of the density and size of stellate hairs and the scale bud number, were skewed. Thus, values of the size, the density + 1, and the number + 1 were log-transformed. The phenotypic values of the eight traits were scaled (mean = 0 and variance = 1) and applied to PCA. Contributions of each principal component (PC) to the total phenotypic variation and loadings of each trait to the first and second PCs were obtained. Statistical differences in PC values among taxa were verified using the function kruskal.test in R 3.3.2.

To evaluate phenotypic plasticity in response to inland and coastal environments, we plotted the *Qd* ancestry and the first phenotypic PC values of individual trees and fitted smoothed lines in each of the inland and coastal sites using the function lowess with the parameter$f = 1$ in R 3.3.2. We applied a linear model to the data using the function lm in R 3.3.2,

$$y \sim \alpha + \beta_1 x_1 + \beta_2 x_2 + \gamma x_1 x_2,$$

where $y$ is the first phenotypic PC value,$x_1$ is the *Qd* ancestry, and$x_2$ is 0 in the inland site and 1 in the coastal site; $\alpha$ is an intercept, $\beta_1$ and $\beta_2$ are coefficients of $x_1$ and $x_2$effects, respectively, and $\gamma$ is a coefficient of their interactions. Significant $\gamma$ indicates different slopes between the sites, suggesting different reaction norms of phenotypic plasticity in response to coastal environment depending on the *Qd* ancestry.

### 2.6 | Tree performance

To show local adaptation of trees with different phenotypes to inland and coastal environments, we plotted the mean values of the first phenotypic PC and the mean values of the stem basal area of all living and dead trees in individual plantation rows and fitted smoothed lines in each of the inland and coastal sites using the function lowess with$f = 1$ in R 3.3.2. We interpreted different slopes of fitted lines between the sites as local adaptation. The stem basal area ($cm^2$) of living trees was calculated from the measured girths of their stems. The stem basal area of dead trees was treated as 0 $cm^2$. Thinned trees in the inland site were excluded from the calculation. Statistical differences in the mean stem basal area among taxa in each site were verified using the function kruskal.test in R 3.3.2.

### 2.7 | Local ancestry and genome-wide patterns of introgression

Haplotypes were estimated from SNP genotypes at ddRAD loci in each chromosome through imputation and phasing using Beagle 5.2 (Browning et al. 2018; Browning et al. 2021). Sampled trees in both sites were divided into *Qc* reference individuals (the *Qd* ancestry$S = 0$), admixed individuals ($0 < S < 1$), and *Qd* reference individuals ($S = 1$). We converted a haplotype matrix in each of three vcf files of the *Qc* reference individuals, the *Qd* reference individuals, and the admixed individuals into a Numpy array using the function vcf2npy. Local ancestry at ddRAD loci of the admixed individuals was described as homozygote of alleles derived from either *Qc* or *Qd*ancestral population and heterozygote of alleles derived from both*Qc* and *Qd* ancestral populations. The three ancestry types were inferred from the haplotype arrays using the Python package Loter with the functions lc.loter_smooth and loter.locanc.local_ancestry (Dias-Alves et

al. 2018). The package assumed that haplotypes of admixed individuals originated from hybridization and recombination of ancestral populations of reference individuals (Dias-Alves et al. 2018). To visualize genome-wide patterns of introgression, we calculated the mean number of alleles derived from *Qd* at each locus in the admixed individuals.

To depict genome-wide introgression patterns in another method, we estimated the Patterson's $D$ statistic at ddRAD loci (Martin et al. 2015). The $D$ statistic requires allele frequencies of four populations with phylogenetic relationship (((P1, P2), P3), O), and positive $D$ values indicate introgression from P3 to P2 as discriminating incomplete lineage sorting. We assigned the *Qc*reference individuals to P1, the admixed individuals to P2, the*Qd* reference individuals to P3, and the *Q. robur* reference sequence to O. We calculated the number of derived alleles that are different from the *Q. robur* reference (ancestral) alleles for individuals of P1, P3, and P3 from the vcf files and obtained the frequency of derived alleles, $p_1$,$p_2$, and $p_3$, respectively, using the package gaston 1.5.9 in R 3.3.2. Using the ABBA-BABA statistics, $C_{\mathrm{ABBA}} = (1 - p_1)\, p_2 p_3$ and $C_{\mathrm{BABA}} = p_1\,(1 - p_2) p_3$, at each locus, we obtained $D = (\Sigma C_{\mathrm{ABBA}} - \Sigma C_{\mathrm{ABBA}}) \,/\, (\Sigma C_{\mathrm{ABBA}} + \Sigma C_{\mathrm{ABBA}})$ at sliding windows of 101 neighboring loci, which sufficiently reduced errors in the calculation of $D$ .

### 2.8 | Association of loci with traits

To detect loci associated with each of the eight traits, we examined genome-wide association (GWA) of SNP genotypes (association mapping) and GWA of local ancestry (admixture mapping) at ddRAD loci with the phenotypic values using mixed linear models. Despite the similarities between association mapping and admixture mapping, some differences between them in terms of aims and methods result in both merits and demerits of each (Buerkle and Lexer 2008). Association mapping can deal with complicated background of ancestry and variation within ancestral lineages underlying phenotypes using more loci densely distributed across a genome, while admixture mapping can work with fewer loci sparsely distributed owing to larger blocks of linkage disequilibrium in recombinants of distinct ancestries (Buerkle and Lexer 2008).

Phenotypic values of individual trees with the same *Qd* ancestry were expected to differ between the inland and coastal sites due to phenotypic plasticity. To exclude such confounding effects with environment and plasticity and to conduct GWA in both sites together, we scaled phenotypic values (mean = 0 and variance = 1) in each site separately and applied a mixed linear model to pooled data of the scaled values in both sites. Environmental heterogeneity within the sites were incorporated as random errors in the models.

To conduct GWA, we used single-locus GWA (Yu et al. 2006) implemented in the package rrBLUP 4.5 (Endelman 2011) in R 3.3.2. To discriminate confounding factors with genetic structure of sampled trees in both sites, we used the Q + K model with a population structure matrix Q calculated from probabilistic principal component analysis using the function ppca in the package pcaMethods (Stacklies et al. 2007) and a kinship matrix K calculated from realized additive relationship using the function A.mat in rrBLUP. The first four principal components were used for the Q matrix. All parameters in the GWA were set at the default values. Significant associations were regarded as $< 0.05$ false discovery rate (FDR) of $-\log_{10} p$ calculated using the function p.adjust in R 3.3.2. Q-Q plots of expected and observed $-\log_{10} p$ values were examined for associations of SNP genotypes and local ancestry.

To search for genes involved in the adaptation to coastal environment around the trait-associated loci, we selected genes (protein ID) nearest to the loci detected by association mapping and within regions including the loci detected by admixture mapping from PM1N v2.3 *Q. robur*annotation database (https://urgi.versailles.inra.fr/OakMine_PM1N) (Plomion et al. 2018). We obtained gene ontology (GO) terms and protein descriptions of the genes.

## 3 | Results

### 3.1 | Genotypes

In the inland site, 575 living and 197 dead trees were found, and 106 trees were sampled from the living trees (Figure S2, Data S1 in Supporting Information). In the coastal site, 350 living and 46 dead trees were found, and 118 trees were sampled from the living trees (Figure S3, Data S1). Taxonomic assemblages of

sampled trees were biased to *Qc* (41 *Qc* , 40 *Qa* , and 25 *Qd* trees) in the inland site and biased to *Qd* (12 *Qc* , 48 *Qa* , and 58 *Qd* trees) in the coastal site probably due to different mortality in inland and coastal habitats (Table S1).

SNP genotypes at 27495 ddRAD loci were obtained from the 224 sampled trees in both sites. Bayesian clustering for SNP genotypes demonstrated a larger increase in log-likelihood from one to two clusters ($K$ = 1–2) and an additional smaller increase from two to three clusters ($K$ = 2–3; Figure S5). When two clusters representing *Qc* and *Qd* were recognized, genetic differentiation based on $F_{ST}$ between these clusters was 0.183. Ancestry proportion of the *Qd* cluster ($Q$ ) was lower in *Qc* trees ($0.00 < Q < 0.17$), intermediate in *Qa* trees ($0.00 < Q < 0.45$), and intermediate or higher in *Qd* trees ($0.23 < Q < 1.00$; Figure S5). These findings suggested that genetic variation mainly existed between *Qc* and *Qd* and that their admixture characterized *Qa* and a part of *Qd* .

For the sampled trees in both sites, the *Qd* ancestry ($S$ ) and inter-ancestry heterozygosity ($H$ ) were estimated from allele frequencies of the *Qc* and *Qd* clusters obtained from the Bayesian clustering. Genomic compositions shown in the coordinates of $S$ and $H$ indicated nearly random admixture between the ancestral populations of *Qc* and *Qd* (Figure 2). In both sites, *Qd* trees from provenances near the distributional limit in the northernmost area of Hokkaido showed lower *Qd* ancestry ($0.23 < S < 0.91$) than those from provenances in the other southern areas ($0.78 < S < 1.00$), and *Qa* trees from coastal provenances north to the distributional limit of *Qd* showed higher *Qd* ancestry ($0.00 < S < 0.45$) than *Qc* trees from inland provenances in Hokkaido ($0.00 < S < 0.06$; Figure 2). These findings suggested a hybrid zone between *Qc* and *Qd* around the northern distributional limit of *Qd* , including both northern-edge *Qd* populations admixed with *Qc* and coastal *Qa* populations backcrossed to *Qc* .

### 3.2 | Phenotypes

Phenotypic values of the eight morphological traits of leaves and shoots were obtained from the 224 sampled trees in the inland and coastal sites (Data S1). PCA for the eight traits summarized the first and second PCs that contributed to 45.2% and 16.7%, respectively, of phenotypic variation (Figure 3a). All the eight traits positively affected the first PC, which represented *Qd* -like phenotypes (Figure 3a). Among the eight traits, four leaf traits (relative leaf width, lateral vein interval, tooth angle, and stellate hair length), namely taxon-specific traits, negatively affected to the second PC. Another two leaf and two shoot traits (stellate hair density, LMA, shoot diameter, and scale bud number), namely habitat-specific traits, positively affected the second PC.

In both sites, *Qc* , *Qa* , and *Qd* trees showed lower, intermediate, and higher first PC values, respectively ($P < 0.001$), and *Qa* and *Qd* trees showed higher and lower second PC values, respectively ($P < 0.001$; Figure 3b, c). Thus, coastal *Qa* trees mainly differed from inland *Qc* trees in the habitat-specific traits, while *Qa* trees mainly differed from *Qd* trees in the taxon-specific traits. Overall, both taxon-specific and habitat-specific traits contributed to phenotypic variation between *Qc* and *Qd* , which was represented by the first PC.

Relationship between the *Qd* ancestry and the first phenotypic PC value differed between the sites, indicating phenotypic plasticity (Figure 4). The first phenotypic PC value was increasing with the *Qd* ancestry ($\beta_1$ = 4.35, $P < 0.001$) and higher in the coastal sites than in the inland site ($\beta_2$ = 2.20, $P < 0.001$). A slope of the first phenotypic PC value to the *Qd* ancestry was more gentler in the coastal site than in the inland site ($\gamma$ = –1.97, $P < 0.001$), indicating larger phenotypic response of *Qa* trees than in *Qd* trees to coastal environment.

### 3.3 | Tree performance

Relationship between the mean first phenotypic PC values and the stem basal area of both living and dead trees in individual plantation rows showed the opposite patterns between the inland and coastal sites (Figure 5), suggesting local adaptation. While the tree size was generally larger in the inland site than in the coastal site, the size of *Qc* trees was extremely reduced in the coastal site, but the size of *Qd* trees was similar in both

sites (Figure 5). The size of *Qa* trees was smaller than that of *Qc* trees ($P = 0.004$) but was not significantly different from that of *Qd* trees ($P = 0.096$) in the inland site, whereas the size of *Qa*trees was larger than that of *Qc* trees ($P = 0.004$) but was not significantly different from that of *Qd* trees ($P = 0.064$) in the coastal site (Data S1). These results suggested that *Qd* -like phenotypes of *Qa* trees in both taxon-specific and habitat-specific traits were adaptive to coastal environment.

### 3.4 | Local ancestry and genome-wide patterns of introgression

Haplotypes at 27495 ddRAD loci in each chromosome were obtained from imputation and phasing for SNP genotypes of the 224 sampled trees in both sites. Among the sampled trees, 47 *Qc* trees (the *Qd*ancestry $S = 0$) and 25 *Qd* trees ($S = 1$) were selected as *Qc* and *Qd* reference individuals, respectively (Table S1). Local ancestry (*Qc* homzygote, *Qc* and *Qd*heterozygote, and *Qd* homozygote) at ddRAD loci in each chromosome was inferred for the remaining 152 admixed individuals based on the haplotypes of the *Qc* and *Qd* reference individuals (Figure 6a). Genome-wide patterns of local ancestry in admixed individuals indicated heterogeneous ancestry along chromosomes (Figure 6b).

The Patterson's *D* statistics obtained at sliding windows of 101 neighboring ddRAD loci were also heterogeneous along chromosomes (Figure S7). Genomic regions showing excessive introgression (higher *D*values; Figures S7) were not always consistent with those with higher local ancestry from *Qd* (Figure 6b).

### 3.5 | Trait-associated loci

Difference in phenotypic values between the inland and coastal sites and dependence of phenotypic values on the *Qd* ancestry varied among the eight traits (Figures S8, S9). Phenotypic values of each trait were scaled in each site separately. Scaled phenotypic values of the 224 sampled trees in both sites were pooled and applied to mixed linear models with effects of genetic structure and kinship relationship. Based on PCA of SNP genotypes at ddRAD loci, genetic variation between *Qc* and *Qd* mainly determined genetic structure in the first PC (Figure S10), and some northern-edge *Qd* populations had unique genetic properties in the second, third, and fourth PCs (Figure S10b–d). Q-Q plots of association mapping of SNP genotypes and admixture mapping of local ancestry showed consistent relationships between expected and observed log-likelihood values at loci with a lower range of $-\log_{10} p$ values, which represented the majority of unassociated loci, indicating successful fitting (Figures S11, S12).

We did not detect any loci significantly associated with the eight traits (FDR $> 0.05$) but found some loci potentially associated with one taxon-specific trait and three habitat-specific traits (0.051 [?] FDR [?] 0.148; Figure 7, Table S2). Association mapping detected three loci in chromosomes 2, 7, and 9 associated with lateral vein interval (Figure 7c), and admixture mapping also supported one locus in chromosome 2 of the three loci (Figure 7d). For loci associated with stellate hair density, association mapping detected one locus in chromosome 1 (Figure 7i), and admixture mapping detected loci in two genomic regions in chromosomes 10 and 11 (Figure 7j). Admixture mapping detected loci associated with LMA in chromosome 11 (Figure 7l), and association mapping detected one locus associated with shoot diameter in chromosome 1 (Figure 7m). Among them, a locus in chromosome 9 potentially associated with lateral vein interval showed a high value of the Patterson's *D* statistics ($D = 0.51$; Figure S7), and a region of loci potentially associated with stellate hair density in chromosome 11 showed high local ancestry from *Qd* (1.33 *Qd*alleles; Figure 6b).

From 31 genes around the loci potentially associated with the four traits, we obtained 39 GO terms, in which most frequently observed terms were DNA binding and protein binding (Table S2). Among the 31 genes, we obtained 10 protein names (Table S2), some of which were related to drought stress resistance (Lorenzo et al. 2002; Kushiro et al. 2004), disease resistance (Van Damme et al. 2009; Mokryakova et al. 2014), and senescence (Engqvist et al. 2011).

## 4 | Discussion

Adaptive introgression is known in some plant taxa, often resulting in divergent ecotypes colonizing novel habitats (Suarez-Gonzalez et al. 2018c). In European and American oaks, divergence and introgression of adaptive traits between interfertile species have been demonstrated. In drought-averse *Q. rubra* and

drought-tolerant *Q. ellipsoidalis* (section *Lobatae* ), parapatric populations of both species are fixed for alternate alleles at a *CONSTANS* -like gene, which affected seedling survival in common gardens, and the *Q. ellipsoidalis* allele is introgressed into the *Q. rubra* genome depending on soil moisture conditions in their sympatric populations (Lind-Riehl et al. 2014; Lind-Riehl and Gailing 2016; Khodwekar and Gailing 2017). In *Q. robur* and *Q. petraea* (section *Quercus* ), introgression from *Q. robur* contributes to divergence among locally adapted *Q. petraea* populations along a gradient of climatic conditions (Leroy et al. 2020). In Asian oaks, introgressed genomic regions were investigated in admixture between *Q. acutissima* and *Q. variabillis* (section *Cerris* ), and admixed populations occupying similar habitats tended to share the same introgressed regions (Fu et al. 2022). We also found a candidate system for adaptive introgression, which consists of *Q. mongolica* var. *crispula* ( *Qc* ) in inland habitats and *Q. dentata* ( *Qd* ) in coastal habitats in northern Japan (Nagamitsu et al. 2019; Nagamitsu et al. 2020). In this system, we tried to verify intensive introgression of *Qd* alleles at loci associated with traits adaptive to coastal environment.

Our previous study demonstrated environment-dependent introgression from *Qd* to *Qc* in coastal habitats, resulting in *Q.* × *angustilepidota* ( *Qa* ), which are hybrids after the first generation of backcross to *Qc* (Nagamitsu et al. 2020). Our present study using a comprehensive tree collection in common gardens revealed a hybrid zone around the northern distributional limit of *Qd* , including both northern-edge *Qd* populations admixed with *Qc* and coastal *Qa* populations backcrossed to *Qc* . The observed genomic compositions indicated random admixture between *Qc* and *Qd* , suggesting frequent gene flow and weak genetic drift. The genotypic PCA indicated that some northern-edge *Qd* populations had unique genetic properties in some PCs with minor contributions to genetic variations, suggesting the presence of weak genetic structure in coastal habitats, probably due to fragmentation of sand dunes and coastal cliffs in the distributional range margins. This hybrid zone is likely to be maintained by the tension zone process (Barton and Hewitt 1985). Near the northern distributional limit of *Qd* , gene flow between *Qc* and *Qd* seems relatively frequent, because their flowering synchrony increases at higher latitudes probably due to shorter periods of growing season (Shimizu et al. 1995). Lower fitness of *Qd* at higher latitudes in comparison to fitness of *Qc* coupled with both lower fitness of *Qc* in coastal habitats and lower fitness of *Qd* in inland habitats may be responsible for natural selection that maintains the tension zone.

Common garden experiments have revealed local adaptation in various traits of oaks (Cavender-Bares and Ramírez-Valiente 2017). Local adaptation of *Qc* to climatic conditions was evident at regional scales (Nagamitsu and Shuri 2021). The size of 30-year-old trees in our common gardens indicated that the size was larger in *Qc* trees than in *Qd* trees in the inland site but larger in *Qd* trees than in *Qc* trees in the coastal site. This result demonstrates both adaptation of *Qc* to inland habitats and adaptation of *Qd* to coastal habitats. Although the plantation density and forest management differed between the sites, smaller tree size in the coastal site than in the inland site suggests higher stress in coastal habitats than in inland habitats. In the coastal site, which was located in north to the northern distributional limit of *Qd* , the size of *Qd* trees seemed to be suppressed and to become similar to the size of *Qa* trees. This result implies that environmental conditions at higher latitudes are maladaptive for *Qd* , which is distributed at lower latitudes than *Qc* . These findings of local adaptation are consistent with natural selection expected from the tension zone process.

Morphological traits of leaves and shoots observed in each site indicated more *Qd* -like phenotypes as the *Qd* ancestry increased, suggesting that these traits have the genetic basis derived from *Qd* . Artificially crossed $F_1$ hybrids between *Qc* and *Qd* exhibited pubescent shoots and intermediate phenotypes of morphological traits of leaves and fruits (Ubukata et al. 1996). These findings are consistent with our observed phenotypes of admixed individuals. We categorized into observed traits into taxon-specific and habitat-specific traits based on the results of phenotypic PCA. The habitat-specific traits, of which phenotypes of *Qa* and *Qd* trees in coastal habitats mainly differed from those of *Qc* trees in inland habitats, included the density of stellate hairs (trichomes) on the lower leaf surface, leaf mass per area (LMA), shoot diameter, and the number of axillary buds at bud-scale scars. These traits seem relevant to the stress tolerance in coastal habitats. Higher water absorption capacity of oak leaves with dense trichomes is advantageous in soils with lower water storage capacity (Fernández et al. 2014). Increased LMA in oaks are commonly observed in response

to higher intensity of drought and light (Sancho-Knapik et al. 2021). More buds at the lower part of shoots, such as bud-scale scars, can compensate for bud mortality at the upper part of shoots caused by salt spray and harsh wind in winter (Asai et al. 1986). These lines of evidence suggest that *Qd* -like phenotypes of the habitat-specific traits are more adaptive in coastal environment. Thus, we expected that *Qd* alleles at loci associated with these traits are more intensively introgressed than those in the genomic background.

The observed shift in phenotypic variation to more *Qd* -like phenotypes from inland to coastal habitats suggests phenotypic plasticity in response to coastal stress. This phenotypic shift was larger in *Qa* trees than in *Qd* trees, indicating lower plasticity in more stress-tolerant *Qd* trees. This result is consistent with our previous findings that phenotypic plasticity in natural populations in response to coastal stress, which was measured by bud mortality, decreased with higher *Qd* ancestry estimated from nuclear microsatellite genotypes (Nagamitsu et al. 2019). Similar features in phenotypic plasticity were evident in Mediterranean oaks, *Q. faginea* , which showed lower morphological and physiological plasticity and more conservative resource-use strategy in populations from drier and colder provenances than in those from mesic and milder provenances (Solé-Medina et al. 2022). The phenotypic shift to more *Qd* -like phenotypes of *Qa* trees may result from induced expression of alleles introgressed from stress-tolerant *Qd* in response to coastal stress.

Introgression from *Qd* to *Qc* was evident from a positive genome-wide estimate of the Patterson's *D* statistic in our previous study (Nagamitsu et al. 2020), and genome-wide patterns of introgression in our present study using more loci indicated that the extent of introgression were heterogeneous along chromosomes. However, extensively introgressed regions were not always consistent with local ancestry, probably due to incomplete linage sorting. To determine introgressed genomic regions precisely, denser SNP loci mapped to reference sequences of both parental taxa are necessary (Ai et al. 2022; Wang et al. 2023). In spite of the low resolution in our present study, the heterogeneity along chromosomes and various admixture patterns among individuals may make our GWA analysis feasible owing to a diverse array of recombinants.

We detected few loci consistently associated with traits in both SNP genotypes and local ancestry, probably due to sparse distribution of the available ddRAD loci, polygenic regulation of the examined traits, and confounding factors with the measured phenotypes. In a model plant, *Oryza sativa* , for example, major genes of some agronomic traits with alleles introgressed between rice varieties were clearly detected from both association mapping using SNP genotypes and admixture mapping using local ancestry (Zhao et al. 2010). In poplar, various traits were measured in a common garden of *Populus trichocarpa* , and associations of SNP genotypes with these traits were examined using 29k genome-wide loci (Mckown et al. 2014a; Mckown et al. 2014b). Introgression of *P. balsamifera* alleles to *P. trichocarpa* genome at some candidate genes around these trait-associated loci were detected using denser loci around these candidate genes (Suarez-Gonzalez et al. 2016). Furthermore, using 1169k loci, additional introgressed regions were found from local ancestry inference and admixture mapping (Suarez-Gonzalez et al. 2018a; Suarez-Gonzalez et al. 2018b). These studies imply that more loci are necessary to detect genes responsible for adaptive traits in our oak system. In spite of the limited power of our present study using 27k loci, we found several loci potentially associated with one taxon-specific and three habitat-specific traits. Two of these loci were located at intensively introgressed regions in chromosomes 9 and 11.

GO terms of genes around the loci potentially associated with the four traits suggest that these genes are related to signaling processes and stress responses with functions of DNA binding and protein binding. Some proteins of those genes were related to catabolic pathways of abscisic acid (ABA) in response to drought stress (Kushiro et al. 2004) and ABA transduction cascades in dormant seeds (Lorenzo et al. 2002), immunophilin responses to bacterial invasion (Mokryakova et al. 2014) and homoserine accumulation triggering pathogen resistance (Van Damme et al. 2009), and catabolism of lysine during leaf senescence (Engqvist et al. 2011). These findings imply that these genes can be related to the response to coastal stress. In introgression between *Q. acutissima* and *Q. variabilis* in China, not only genes involved in signaling processes such as responses to abiotic stimulus, stress, hormone, and pathogens but also *cis* -regulatory elements in untranslated regions were enriched in introgressed genomic regions (Fu et al. 2022). To detect candidate genes responsible for the *Qd* -like phenotypes in response to coastal stress, not only morphological and physiological traits but

also gene expression patterns should be investigated to select essential transcription factors and regulatory elements underlying adaptive phenotypes.

In summary, we revealed a hybrid zone with random admixture between *Qc* and *Qd* in the northernmost area of Hokkaido. This hybrid zone is located in coastal habitats around the northern distributional limit of *Qd* , where *Qd* -like phenotypes are adaptive. We found heterogeneity of introgression along chromosomes and various admixture patterns among individuals, but failed to detect loci associated with the *Qd* -like phenotypes. To elucidate adaptive introgression suggested in our present study, more SNP genotypes at denser loci in admixed populations and deeper knowledge of genetic basis of adaptive traits are necessary.

**Acknowledgements**

We thank Kazuhito Kita and Nobuhiro Akashi (Hokkaido Research Organization) for their help to investigate the inland and coastal sites; Atsushi Nakanishi and Keiko Kitamura (Forest Research and Management Organization) for their cooperation of the investigation; Akiko Takazawa and Yasuyuki Komatsu for their assistance in the laboratory work; Mineaki Aizawa (Utsunomiya University), and Ichiro Tamaki (Gifu Prefectural Research Institute for Forests) for their suggestions for improving the manuscript.

**Author contributions**

TN conceived the study. HS provided the inland and coastal sites. TN, KU, and AI obtained and analyzed the data. TN drafted the manuscript. KU, AI, and HS revised the manuscript.

**Conflict of Interest Statement**

The authors declare no conflict of interest.

**Funding Information**

This study was supported by JSPS KAKENHI grant no. 17K07859 to TN.

**Data Accessibility Statement**

The data of phenotypes and performance of trees in the common gardens are given in Supporting Information (Data S1).

**References**

Ai W, Liu Y, Mei M, et al (2022) A chromosome-scale genome assembly of the Mongolian oak (Quercus mongolica). Molecular Ecology Resources 22:2396–2410. doi: 10.1111/1755-0998.13616

Aizawa M, Maekawa K, Mochizuki H, Iizuka K (2021) Taxonomic revision of quercus serrata subsp. mongolicoides. Acta Phytotaxonomica et Geobotanica 72:113–123. doi: 10.18942/apg.202017

Alexander DH, Lange K (2011) Enhancements to the ADMIXTURE algorithm for individual ancestry estimation. BMC Bioinformatics 12:246. doi: 10.1186/1471-2105-12-246

Anderson E (1953) Introgressive hybridization. Biological reviews of the Cambridge Philosophical Society 28:280–307.

Anderson E, Stebbins GL (1954) Hybridization as an evolutionary stimulus. Evolution 8:378–388.

Arnold BJ, Lahner B, DaCosta JM, et al (2016) Borrowed alleles and convergence in serpentine adaptation. Proceedings of the National Academy of Sciences of the United States of America 113:8320–8325. doi: 10.1073/pnas.1600405113

Asai T, Shinmura Y, Usui G (1986) Mortality factor of the winter buds of Quercus dentata and Quercus mongolica var. grosseserrata in natural coastal forests of northern Hokkaido. Journal of Japanese Forest Society 68:368–374. doi: 10.11519/jjfs1953.68.9_368

Barton NH, Hewitt GM (1985) Analysis of hybrid zones. Annual Review of Ecology and Systematics 16:113–148. doi: 10.1146/annurev.es.16.110185.000553

Bickford CP (2016) Ecophysiology of leaf trichomes. Functional Plant Biology 43:807–814. doi: 10.1071/FP16095

Bresadola L, Caseys C, Castiglione S, et al (2019) Admixture mapping in interspecific Populus hybrids identifies classes of genomic architectures for phytochemical, morphological and growth traits. New Phytologist 223:2076–2089. doi: 10.1111/nph.15930

Browning BL, Tian X, Zhou Y, Browning SR (2021) Fast two-stage phasing of large-scale sequence data. The American Journal of Human Genetics 108:1880–1890. doi: 10.1016/j.ajhg.2021.08.005

Browning BL, Zhou Y, Browning SR (2018) A one-penny imputed genome from next-generation reference panels. American Journal of Human Genetics 103:338–348. doi: 10.1016/j.ajhg.2018.07.015

Buerkle CA, Lexer C (2008) Admixture as the basis for genetic mapping. Trends in Ecology and Evolution 23:686–694. doi: 10.1016/j.tree.2008.07.008

Burke JM, Arnold ML (2001) Genetics and the fitness of hybrids. Annual Review of Genetics 35:31–52.

Cavender-Bares J (2019) Diversification, adaptation, and community assembly of the American oaks (Quercus), a model clade for integrating ecology and evolution. New Phytologist 221:669–692. doi: 10.1111/nph.15450

Cavender-Bares J, Ramirez-Valiente JA (2017) Physiological evidence from common garden experiments for local adaptation and adaptive plasticity to climate in American live oaks (Quercus section Virentes): Implications for conservation under global change. In: Gil-Pelegrin E, Peguero-Pina J, Sancho-Knapik D (eds) Oaks Physiological Ecology. Exploring the Functional Diversity of Genus Quercus L. Tree Physiology, vol 7. Springer, Cham, pp 107–135

Chhatre VE, Evans LM, DiFazio SP, Keller SR (2018) Adaptive introgression and maintenance of a trispecies hybrid complex in range-edge populations of Populus. Molecular Ecology 27:4820–4838. doi: 10.1111/mec.14820

Ciccarelli D, Bona C (2022) Exploring the functional strategies adopted by coastal plants along an ecological gradient using morpho-functional traits. Estuaries and Coasts 45:114–129. doi: 10.1007/s12237-021-00945-y

Danecek P, Auton A, Abecasis G, et al (2011) The variant call format and VCFtools. Bioinformatics 27:2156–2158. doi: 10.1093/bioinformatics/btr330

Denk T, Grimm GW, Manos PS, et al (2017) An updated infrageneric classification of the oaks: review of previous taxonomic schemes and synthesis of evolutionary patterns. In: Oaks Physiological Ecology. Exploring the Functional Diversity of Genus Quercus.

Dias-Alves T, Mairal J, Blum MGB (2018) Loter: A software package to infer local ancestry for a wide range of species. Molecular Biology and Evolution 35:2318–2326. doi: 10.1093/molbev/msy126

Endelman JB (2011) Ridge regression and other kernels for genomic selection with R package rrBLUP. The Plant Genome 4:250–255. doi: 10.3835/plantgenome2011.08.0024

Engqvist MKM, Kuhn A, Wienstroer J, et al (2011) Plant D-2-hydroxyglutarate dehydrogenase participates in the catabolism of lysine especially during senescence. Journal of Biological Chemistry 286:11382–11390. doi: 10.1074/jbc.M110.194175

Fernandez V, Sancho-Knapik D, Guzman P, et al (2014) Wettability, polarity, and water absorption of holm oak leaves: Effect of leaf side and age. Plant Physiology 166:168–180. doi: 10.1104/pp.114.242040

Fitzpatrick BM (2012) Estimating ancestry and heterozygosity of hybrids using molecular markers. BMC Evolutionary Biology 12:131. doi: 10.1186/1471-2148-12-131

Fu R, Zhu Y, Liu Y, et al (2022) Genome-wide analyses of introgression between two sympatric Asian oak species. Nature Ecology & Evolution 6:924–935. doi: 10.1038/s41559-022-01754-7

Goulet BE, Roda F, Hopkins R (2017) Hybridization in plants: Old ideas, new techniques. Plant Physiology 173:65–78. doi: 10.1104/pp.16.01340

Hamilton JA, Miller JM (2016) Adaptive introgression as a resource for management and genetic conservation in a changing climate. Conservation Biology 30:33–41. doi: 10.1111/cobi.12574

Hesp PA (1991) Ecological processes and plant adaptations on coastal dunes. Journal of Arid Environments 21:165–191. doi: 10.1016/S0140-1963(18)30681-5

Hipp AL, Manos PS, Hahn M, et al (2020) Genomic landscape of the global oak phylogeny. New Phytologist 226:1198–1212. doi: 10.1111/nph.16162

Ishida TA, Hattori K, Sato H, Kimura MT (2003) Differentiation and hybridization between Quercus crispula and Q. dentata (Fagaceae): Insights from morphological traits, amplified fragment length polymorphism markers, and leafminer composition. American Journal of Botany 90:769–776. doi: 10.3732/ajb.90.5.769

Khodwekar S, Gailing O (2017) Evidence for environment-dependent introgression of adaptive genes between two red oak species with different drought adaptations. American Journal of Botany 104:1088–1098. doi: 10.3732/ajb.1700060

Kim BY, Wei X, Fitz-Gibbon S, et al (2018) RADseq data reveal ancient, but not pervasive, introgression between Californian tree and scrub oak species (Quercus sect. Quercus, Fagaceae). Molecular Ecology 27:4556–4571. doi: 10.1111/mec.14869

Kushiro T, Okamoto M, Nakabayashi K, et al (2004) The Arabidopsis cytochrome P450 CYP707A encodes ABA 8'-hydroxylases: Key enzymes in ABA catabolism. EMBO Journal 23:1647–1656. doi: 10.1038/sj.emboj.7600121

Leroy T, Louvet JM, Lalanne C, et al (2020) Adaptive introgression as a driver of local adaptation to climate in European white oaks. New Phytologist 226:1171–1182. doi: 10.1111/nph.16095

Lind-Riehl J, Gailing O (2016) Adaptive variation and introgression of a CONSTANS-like gene in North American red oaks. Forests 8:3. doi: 10.3390/f8010003

Lind-Riehl JF, Sullivan AR, Gailing O (2014) Evidence for selection on a CONSTANS-like gene between two red oak species. Annals of Botany 113:967–975. doi: 10.1093/aob/mcu019

Lindtke D, Gonzalez-Martinez SC, Macaya-Sanz D, Lexer C (2013) Admixture mapping of quantitative traits in Populus hybrid zones: Power and limitations. Heredity 111:474–485. doi: 10.1038/hdy.2013.69

Lorenzo O, Nicolas C, Nicolas G, Rodriguez D (2002) Molecular cloning of a functional protein phosphatase 2C (FsPP2C2) with unusual features and synergistically up-regulated by ABA and calcium in dormant seeds of Fagus sylvatica. Physiologia Plantarum 114:482–490. doi: 10.1034/j.1399-3054.2002.1140318.x

Ma Y, Wang J, Hu Q, et al (2019) Ancient introgression drives adaptation to cooler and drier mountain habitats in a cypress species complex. Communications Biology 2:213. doi: 10.1038/s42003-019-0445-z

Martin NH, Bouck AC, Arnold ML (2006) Detecting adaptive trait introgression between Iris fulva and I. brevicaulis in highly selective field conditions. Genetics 172:2481–2489. doi: 10.1534/genetics.105.053538

Martin SH, Davey JW, Jiggins CD (2015) Evaluating the use of ABBA-BABA statistics to locate introgressed loci. Molecular Biology and Evolution 32:244–257. doi: 10.1093/molbev/msu269

Martin SH, Van Belleghem SM (2017) Exploring evolutionary relationships across the genome using topology weighting. Genetics 206:429–438. doi: 10.1534/genetics.116.194720

Matsumoto A, Kawahara T, Kanazashi A, et al (2009) Differentiation of three closely related Japanese oak species and detection of interspecific hybrids using AFLP markers. Botany 87:145–153. doi: 10.1139/B08-121

Mckown AD, Guy RD, Klapště J, et al (2014a) Geographical and environmental gradients shape phenotypic trait variation and genetic structure in Populus trichocarpa. New Phytologist 201:1263–1276. doi: 10.1111/nph.12601

Mckown AD, Klápště J, Guy RD, et al (2014b) Genome-wide association implicates numerous genes underlying ecological trait variation in natural populations of Populus trichocarpa. New Phytologist 203:535–553. doi: 10.1111/nph.12815

Menon M, Bagley JC, Page GFM, et al (2021) Adaptive evolution in a conifer hybrid zone is driven by a mosaic of recently introgressed and background genetic variants. Communications Biology 4:1–14. doi: 10.1038/s42003-020-01632-7

Mokryakova M V., Pogorelko G V., Bruskin SA, et al (2014) The role of peptidyl-prolyl cis/trans isomerase genes of Arabidopsis thaliana in plant defense during the course of Xanthomonas campestris infection. Russian Journal of Genetics 50:140–148. doi: 10.1134/S1022795414020100

Nagamitsu T, Shimizu H, Aizawa M, Nakanishi A (2019) An admixture of Quercus dentata in the coastal ecotype of Q. mongolica var. crispula in northern Hokkaido and genetic and environmental effects on their traits. Journal of Plant Research 132:211–222. doi: 10.1007/s10265-018-01079-2

Nagamitsu T, Shuri K (2021) Seed transfer across geographic regions in different climates leads to reduced tree growth and genetic admixture in Quercus mongolica var. crispula. Forest Ecology and Management 482:118787. doi: 10.1016/j.foreco.2020.118787

Nagamitsu T, Uchiyama K, Izuno A, et al (2020) Environment-dependent introgression from Quercus dentata to a coastal ecotype of Quercus mongolica var. crispula in northern Japan. New Phytologist 226:1018–1028. doi: 10.1111/nph.16131

Ohba H (2006) Fagaceae. In: Iwatsuki K, Boufford DE, Ohba H (eds) Flora of Japan. Volume IIa. Kodansha, Tokyo, pp 42–60

Ortego J, Gugger PF, Riordan EC, Sork VL (2014) Influence of climatic niche suitability and geographical overlap on hybridization patterns among southern Californian oaks. Journal of Biogeography 41:1895–1908. doi: 10.1111/jbi.12334

Peterson BK, Weber JN, Kay EH, et al (2012) Double digest RADseq: An inexpensive method for de novo SNP discovery and genotyping in model and non-model species. PLoS ONE 7:e37135. doi: 10.1371/journal.pone.0037135

Petit RJ, Bodénès C, Ducousso A, et al (2004) Hybridization as a mechanism of invasion in oaks. New Phytologist 161:151–164. doi: 10.1046/j.1469-8137.2003.00944.x

Plomion C, Aury JM, Amselem J, et al (2018) Oak genome reveals facets of long lifespan. Nature Plants 4:440–452. doi: 10.1038/s41477-018-0172-3

Puritz JB, Hollenbeck CM, Gold JR (2014) dDocent: a RADseq, variant-calling pipeline designed for population genomics of non-model organisms. PeerJ 2:e431. doi: 10.7717/peerj.431

R_Core_Team (2019) A language and environment for statistical computing. R Foundation for Statistical Computing

Ramírez-Valiente JA, Sánchez-Gómez D, Aranda I, Valladares F (2010) Phenotypic plasticity and local adaptation in leaf ecophysiological traits of 13 contrasting cork oak populations under different water availabilities. Tree Physiology 30:618–627. doi: 10.1093/treephys/tpq013

Rendón-Anaya M, Wilson J, Sveinsson S, et al (2021) Adaptive introgression facilitates adaptation to high latitudes in European aspen (Populus tremula L.). Molecular Biology and Evolution 38:5034–5050. doi: 10.1093/molbev/msab229

Rieseberg LH, Buerkle CA (2002) Genetic mapping in hybrid zones. American Naturalist 159:S37–S50. doi: 10.2307/3078920

Rieseberg LH, Carney SE (1998) Plant hybridization. New Phytologist 140:599–624. doi: 10.1046/j.1469-8137.1998.00315.x

Rieseberg LH, Kim S-C, Randell RA, et al (2007) Hybridization and the colonization of novel habitats by annual sunflowers. Genetica 129:149–165. doi: 10.1007/s10709-006-9011-y

Riordan EC, Gugger PF, Ortego J, et al (2016) Association of genetic and phenotypic variability with geography and climate in three southern California oaks. American Journal of Botany 103:73–85. doi: 10.3732/ajb.1500135

Sancho-Knapik D, Escudero A, Mediavilla S, et al (2021) Deciduous and evergreen oaks show contrasting adaptive responses in leaf mass per area across environments. New Phytologist 230:521–534. doi: 10.1111/nph.17151

Shimizu H, Kikuchi K, Yamada K (1995) Local variation of bud number on axillary buds of bud-scales of Quercus dentata in coastal forest along Japan sea of Hokkaido. Trans Hokkaido Branch Jpn For Soc 43:140–142.

Solé-Medina A, Robledo-Arnuncio JJ, Ramírez-Valiente JA (2022) Multi-trait genetic variation in resource-use strategies and phenotypic plasticity correlates with local climate across the range of a Mediterranean oak (Quercus faginea). New Phytologist 234:462–478. doi: 10.1111/nph.17968

Sork VL (2018) Genomic studies of local adaptation in natural plant populations. Journal of Heredity 109:3–15. doi: 10.1093/jhered/esx091

Sork VL, Cokus SJ, Fitz-Gibbon ST, et al (2022) High-quality genome and methylomes illustrate features underlying evolutionary success of oaks. Nature Communications 13:1–15. doi: 10.1038/s41467-022-29584-y

Sork VL, Riordan E, Gugger PF, et al (2016) Phylogeny and introgression of California scrub white oaks (Quercus section Quercus). International Oaks 27:1–14.

Stacklies W, Redestig H, Scholz M, et al (2007) pcaMethods: A bioconductor package providing PCA methods for incomplete data. Bioinformatics 23:1164–1167. doi: 10.1093/bioinformatics/btm069

Stebbins GL, Matzke EB, Epling C (1947) Hybridization in a population of Quercus marilandica and Quercus ilicifolia. Evolution 1:79. doi: 10.2307/2405406

Suarez-Gonzalez A, Hefer CA, Christe C, et al (2016) Genomic and functional approaches reveal a case of adaptive introgression from Populus balsamifera (balsam poplar) in P. trichocarpa (black cottonwood). Molecular Ecology 25:2427–2442. doi: 10.1111/mec.13539

Suarez-Gonzalez A, Hefer CA, Lexer C, et al (2018a) Introgression from Populus balsamifera underlies adaptively significant variation and range boundaries in P. trichocarpa. New Phytologist 217:416–427. doi: 10.1111/nph.14779

Suarez-Gonzalez A, Hefer CA, Lexer C, et al (2018b) Scale and direction of adaptive introgression between black cottonwood (Populus trichocarpa) and balsam poplar (P. balsamifera). Molecular Ecology 27:1667–1680. doi: 10.1111/mec.14561

Suarez-Gonzalez A, Lexer C, Cronk QCB (2018c) Adaptive introgression: A plant perspective. Biology Letters 14:20170688. doi: 10.1098/rsbl.2017.0688

Ubukata M, Koono K, Iizuka K (1996) Morphological characteristics of Quercus crispula x dentata hybrids. Trans Hokkaido Branch Jpn For Soc 44:113–116.

Van Damme M, Zeilmaker T, Elberse J, et al (2009) Downy mildew resistance in arabidopsis by mutation of Homoserine Kinase. Plant Cell 21:2179–2189. doi: 10.1105/tpc.109.066811

Wang W, He X, Yan X, et al (2023) Chromosome-scale genome assembly and insights into the metabolome and gene regulation of leaf color transition in an important oak species, Quercus dentata. New Phytologist 238:2016–2032. doi: 10.1111/nph.18814

Whitney KD, Randell RA, Rieseberg LH (2010) Adaptive introgression of abiotic tolerance traits in the sunflower Helianthus annuus. New Phytologist 187:230–239. doi: 10.1111/j.1469-8137.2010.03234.x

Yu J, Pressoir G, Briggs WH, et al (2006) A unified mixed-model method for association mapping that accounts for multiple levels of relatedness. Nature Genetics 38:203–208. doi: 10.1038/ng1702

Zhao K, Wright M, Kimball J, et al (2010) Genomic diversity and introgression in O. sativa reveal the impact of domestication and breeding on the rice genome. PLoS ONE 5:e10780. doi: 10.1371/journal.pone.0010780

Table and Figure Legend

**Figure 1.** Locations of provenances of *Quercus mongolica*var. *crispula* (*Qc* , red), *Q.* x*angustilepidota* (green), and *Q. dentata* (*Qd* , blue), which were planted in the inland site (a) and the coastal site (b). Provenances are categorized into southwestern (inverse triangles), northwestern (triangles), northern (diamonds), eastern (squares) districts of the northernmost area of Hokkaido and other areas of Hokkaido (circles). Enlarged symbols indicate reference individuals of*Qc* and *Qd* for inferring local ancestry. Locations of the inland site (red arrow head) and the coastal site (blue arrow head) are shown.

**Figure 2.** *Quercus dentata* ancestry ($S$ ) and inter-ancestry heterozygosity ($H$ ) of sampled trees in the inland site (a) and the coastal site (b). Ancestral populations of *Q. mongolica* var. *crispula* are $S = 0$ and $H = 0$, and those of *Q. dentata* are $S = 0$ and $H = 0$. Solid lines indicate backcrossing from $F_1$ hybrids ($S = 0.5$ and $H = 1$) to ancestral populations, and a dotted curve indicate random mating between the ancestral populations. Symbols are shown in the same way as Figure 1.

**Figure 3.** Principal component analysis for phenotypes of eight morphological traits of leaves and shoots. Proportion (%) of variances for the first five principal components (PCs) and vectors (arrows) of the traits contributing to the first and second PCs are shown (a). Coordination of sampled trees in the inland site (b) and the coastal site (c) on the first and second PCs are shown. Symbols are shown in the same way as Figure 1.

**Figure 4.** Relationship between *Quercus dentata* ancestry and the first principal component of phenotypic variation of sampled trees in the inland site (a) and the coastal site (b). Solid and dotted lines are fitted to observations in the focal site and the other site, respectively, using the lowess method. Symbols are shown in the same way as Figure 1.

**Figure 5.** Relationship between mean values of the first principal component of phenotypic variation of sampled trees and mean values of the stem basal area of recorded trees at plantation rows in the inland site (a) and the coastal site (b). Solid and dotted lines are fitted to observations in the focal site and the other site, respectively, using the lowess method. Symbols are shown in the same way as Figure 1.

**Figure 6.** Genome-wide patterns of local ancestry (a) and mean number of *Quercus dentata* alleles in admixed individuals (b). Along vertical axis (a), *Q. dentata* reference individuals (white), admixed individuals sorted by *Quercus dentata* ancestry, and *Q. mongolica* var. *crispula* reference individuals (black) are arranged. White, black, and grey bars (a) indicate homozygote of *Q. dentata* alleles, homozygote of *Q. mongolica* var. *crispula* alleles, and heterozygote of both alleles, respectively, in admixed individuals. Blue vertical lines indicate borders of chromosomes, and red vertical lines indicate positions of loci potentially associated with traits shown in Figure 7 and Table S2.

**Figure 7.** Manhattan plots of likelihood of genome-wide association with eight morphological traits of leaves and shoots. Left panels (a, c, e, g, i, k, m, o) are association of SNP genotypes (association mapping), and right panels (b, d, f, h, j, l, n, p) are association of local ancestry (admixture mapping). Taxon-specific traits: relative lead width (a, b), lateral vein interval (c, d), tooth angle (e, f), and stellate hair length (g, h); and habitat-specific traits: stellate hair density (i, j), leaf mass per area (k, l), shoot diameter (m, n), and scale bud number (o, p) are shown. Black and grey circles indicate loci in different chromosomes, and green circles indicate loci potentially associated with traits (FDR $< 0.15$).

Supporting Information

Table S1. Provenances of sampled trees in inland and coastal sites.

Figure S1. Photographs of inland site (a) and coastal site (b) in 2017.

Figure S2. Locations and sizes of trees planted in three blocks (a–c) in inland site. Solid circles, circles with crosses, and open circles indicate sampled reference, sampled non-reference, and non-sampled living trees, respectively. Crosses, + and x, indicate dead and thinned trees, respectively. Triangles indicate non-experimental trees. Colors indicate taxa: *Quercus mongolica* var. *crispula* (red),*Q.* x *angustilepidota* (green), and *Q. dentata*(blue).

Figure S3. Locations and sizes of trees planted in two blocks (a, b) in coastal site. Solid circles, circles with crosses, and open circles indicate sampled reference, sampled non-reference, and non-sampled living trees, respectively. Crosses, + and x, indicate dead and thinned trees, respectively. Triangles indicate non-experimental trees. Colors indicate taxa: *Quercus mongolica* var. *crispula* (red),*Q.* x *angustilepidota* (green), and *Q. dentata*(blue).

Figure S4. Measurements for morphological traits of leaves and shoots.

Figure S5. Bayesian clustering of SNP genotypes at ddRAD loci of sampled trees in both inland and coastal sites. Log likelihood when the number of clusters ($K$ ) are 1, 2, and 3 (a). Genetic differentiation ($F_{ST}$) between clusters when $K = 2$ and$K = 3$ (b). Bar plots of ancestry proportions of trees sorted by the ancestry proportion of clusters, when $K = 2$ (c) and $K = 3$ (d). Colors correspond to clusters (b, c, d). Colors of circles indicate taxa: *Quercus mongolica* var. *crispula* (red),*Q.* x *angustilepidota* (green), and *Q. dentata*(blue), and enlarged symbols indicate reference samples (e).

Figure S6. Frequency distributions (scatter plots) and correlations (histograms) for pairs of shoot hair (0: absent and 1: present) and eight morphological traits: relative leaf width, lateral vein interval (mm), tooth angle (@), loge length (mm) and $\log_e$ density ($mm^{-2}$) of stellate hair on lower leaf surface, lead mass per area (mg $mm^{-2}$), shoot diameter (mm), and $\log_e$ number of axillary buds at bud-scale scars. Numbers indicate Kendall's correlation coefficients, and red lines indicate linear regression lines.

Figure S7. Patterson's $D$ statistics at neighboring 101 ddRAD loci along chromosomes. Positive $D$ values indicate introgression from*Quercus dentata* to *Q. mongolica* var. *crispula* . Red vertical lines indicate positions of trait-associated loci shown in Figure 7 and Table S2.

Figure S8. Phenotypic values of four taxon-specific traits in inland (left) and coastal (middle) sites and those values scaled in each site and pooled together (right) in relation to *Quercus dentata*ancestry. Solid and dotted lines are fitted to observations in the focal site and the other site, respectively, using the lowess method. Symbols are shown in the same way as Figure 1.

Figure S9. Phenotypic values of four habitat-specific traits in inland (left) and coastal (middle) sites and those values scaled in each site and pooled together (right) in relation to *Quercus dentata*ancestry. Solid and dotted lines are fitted to observations in the focal site and the other site, respectively, using the lowess method. Symbols are shown in the same way as Figure 1.

Figure S10. Principal component analysis for SNP genotypes at ddRAD loci of sampled trees in both inland and coastal sites. Proportion (%) of variances for the first 10 principal components (PCs) are shown (a).

Coordination of sampled trees on the first and second PCs (b), the first and third PCs (c), and the first and fourth PCs (d) are shown. Symbols are shown in the same way as Figure 1.

Figure S11. Q-Q plots of expected and observed $-\log_{10}p$ values for four taxon-specific traits. Red lines indicate identical expected and observed $-\log_{10}\ p$ values.

Figure S12. Q-Q plots of expected and observed $-\log_{10}p$ values for four habitat-specific traits. Red lines indicate identical expected and observed $-\log_{10}\ p$ values.

Table S2. ddRAD loci of SNP genotypes (G) and local ancestry (A) associated with traits (FDR $< 0.15$) and proteins nearest to or between trait-associated loci obtained from PM1N v2.3 *Quercus robur* annotation database.

Data S1. Data of phenotypes of morphological traits of leaves and shoots and performance of trees in plantation rows in inland and coastal common gardens.

Figure 1

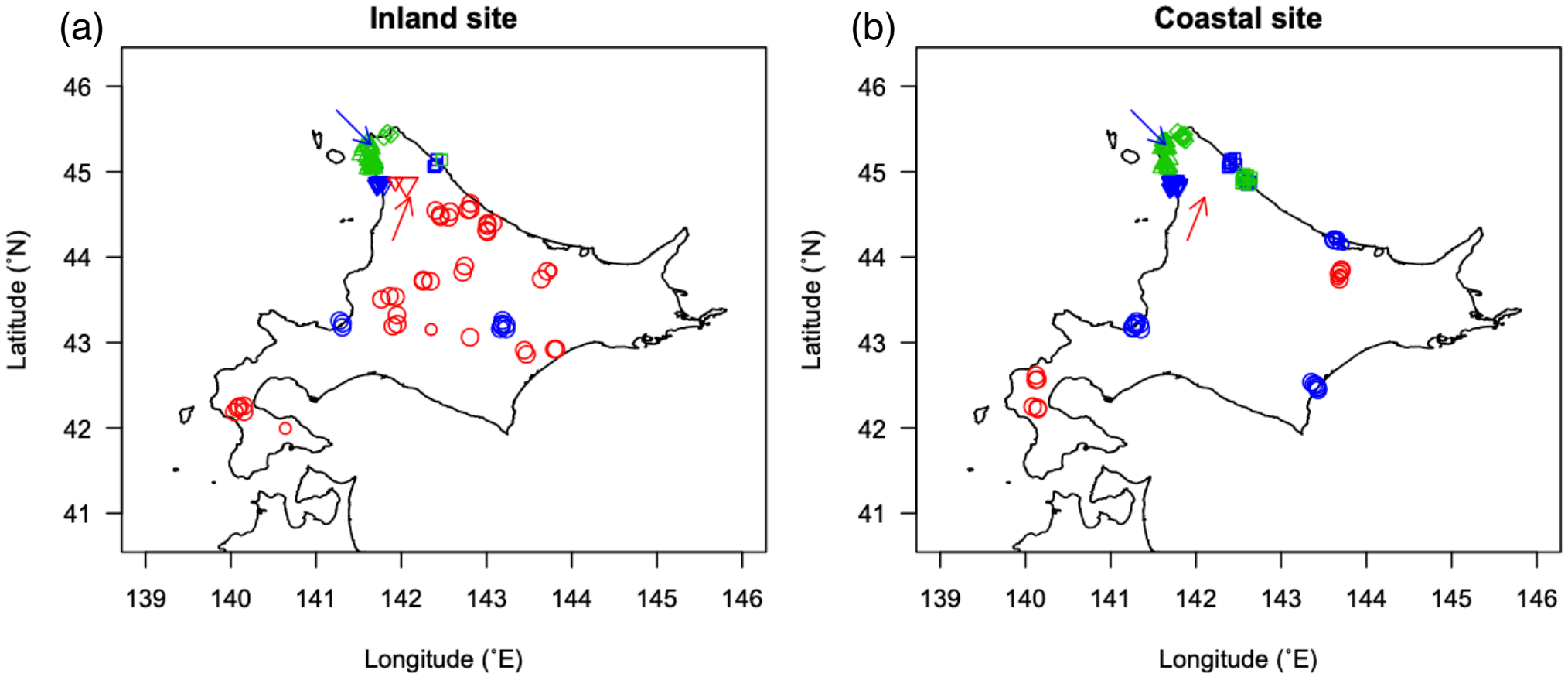
(a)
Inland site
(b)
Coastal site
Latitude (˚N)
Longitude (˚E)
46
45
44
43
42
41
139
140
141
142
143
144
145
146

Figure 2

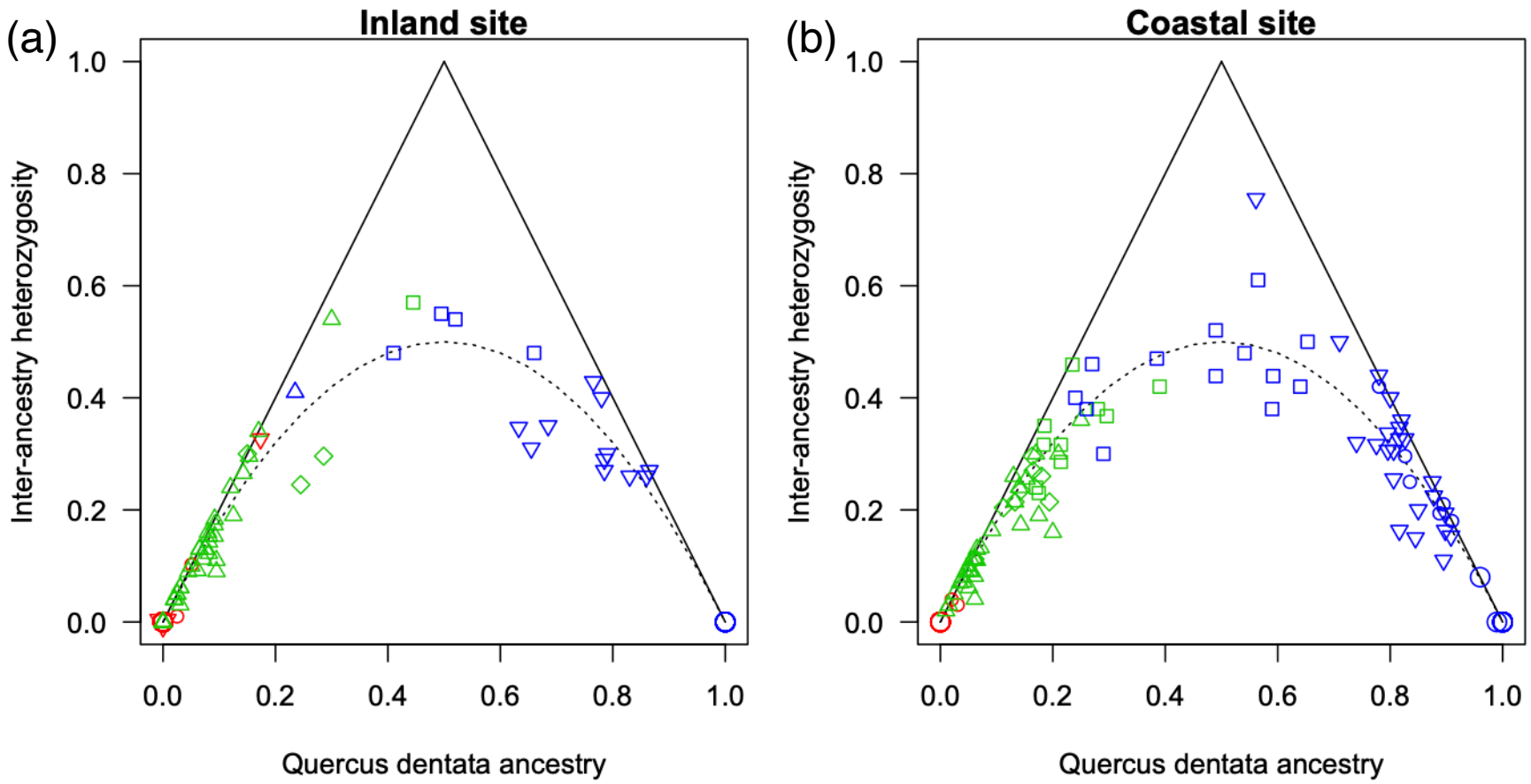
(a)
Inland site
(b)
Coastal site
Inter-ancestry heterozygosity
Quercus dentata ancestry
0.0
0.2
0.4
0.6
0.8
1.0

Figure 3

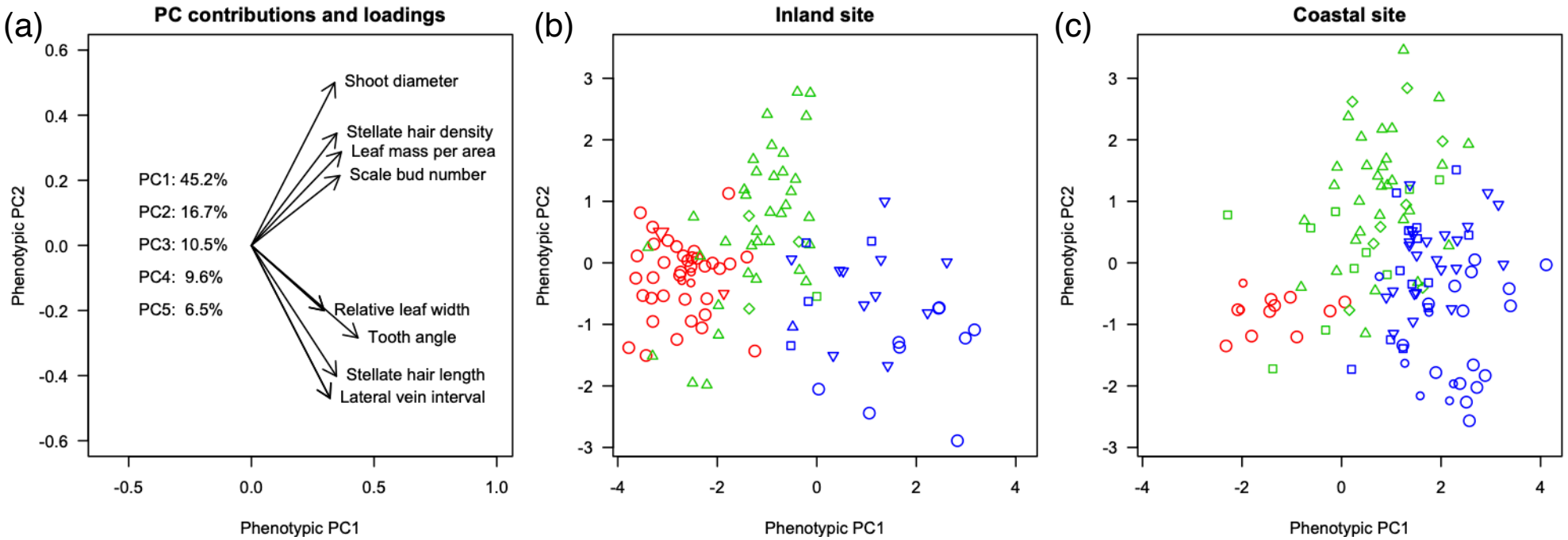
(a)
PC contributions and loadings
Shoot diameter
Stellate hair density
Leaf mass per area
Scale bud number
PC1: 45.2%
PC2: 16.7%
PC3: 10.5%
PC4: 9.6%
PC5: 6.5%
Relative leaf width
Tooth angle
Stellate hair length
Lateral vein interval
Phenotypic PC2
Phenotypic PC1
(b)
Inland site
Phenotypic PC2
Phenotypic PC1
(c)
Coastal site
Phenotypic PC2
Phenotypic PC1

Figure 4

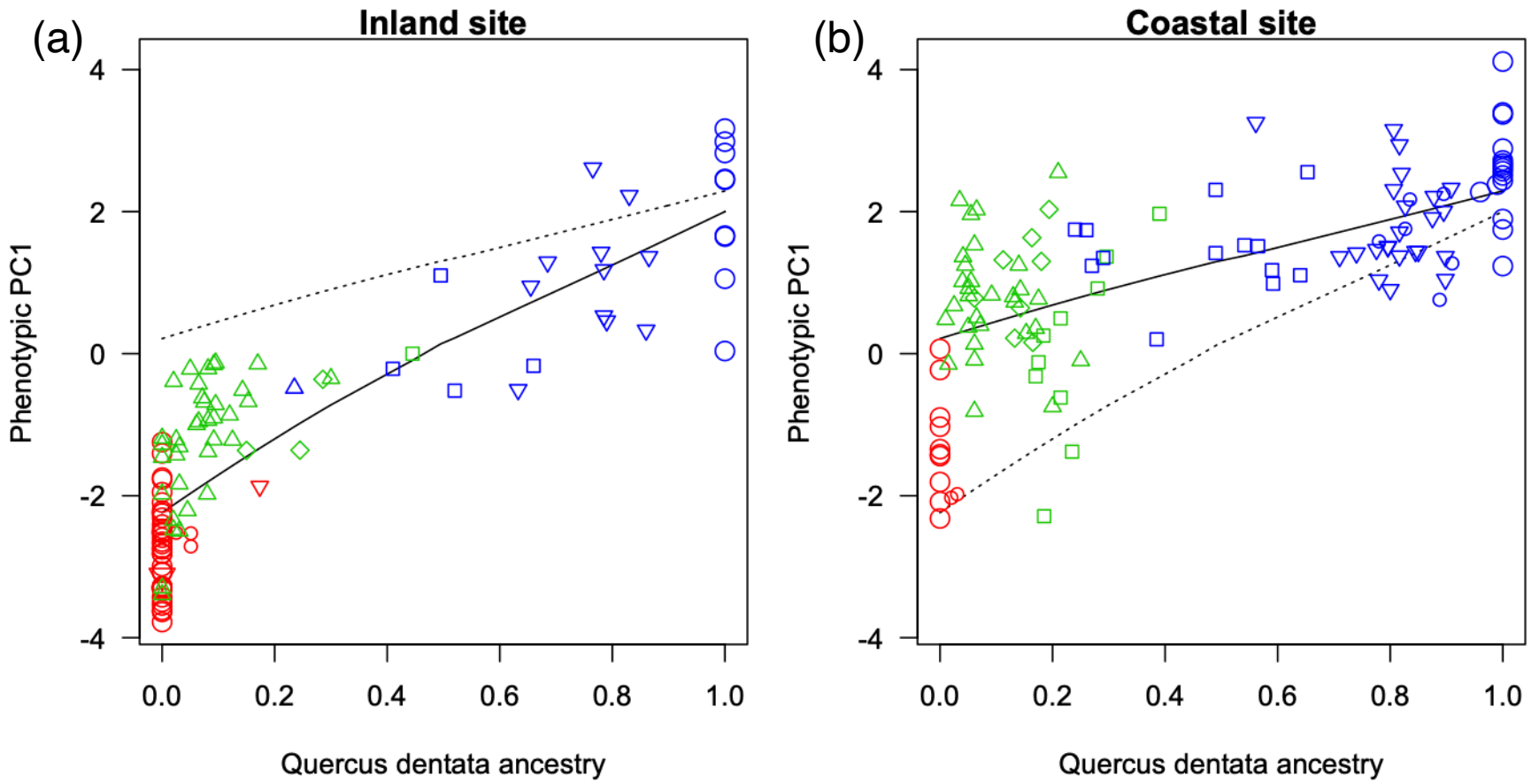
(a)
Inland site
Phenotypic PC1
Quercus dentata ancestry
(b)
Coastal site
Phenotypic PC1
Quercus dentata ancestry

Figure 5

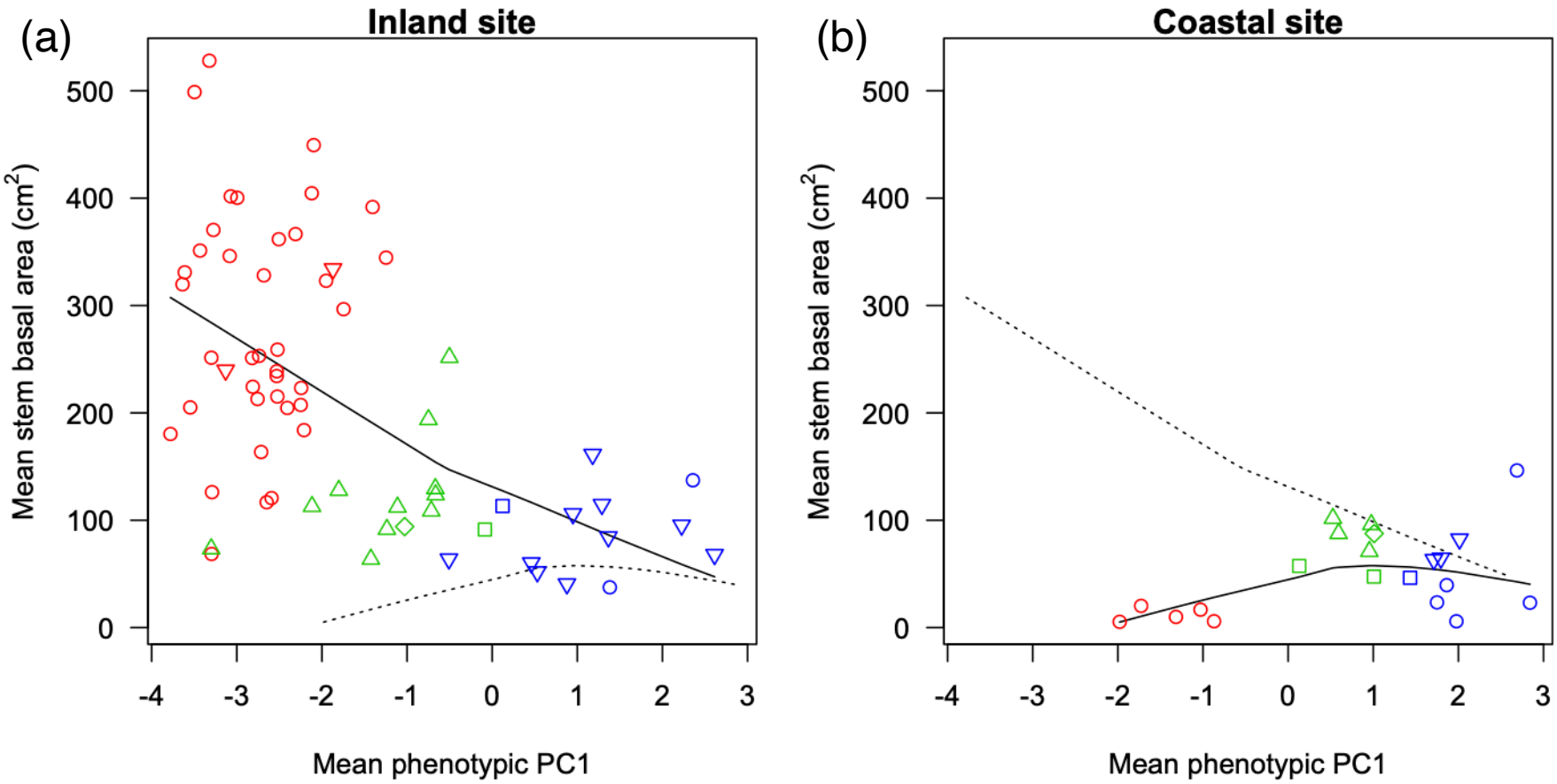
(a)
Inland site
(b)
Coastal site
Mean stem basal area (cm$^2$)
Mean phenotypic PC1
500
400
300
200
100
0
-4
-3
-2
-1
0
1
2
3

Figure 6

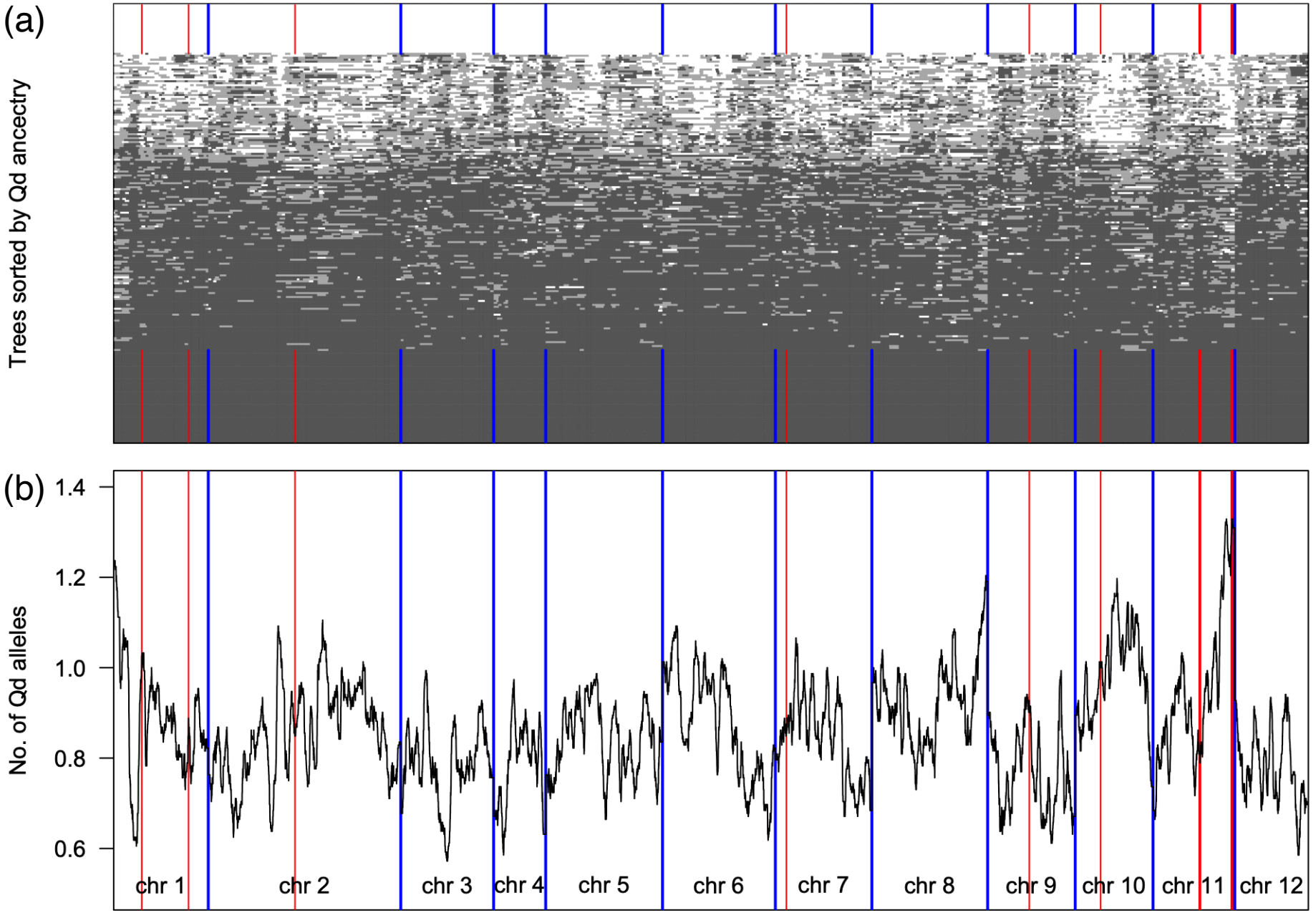
(a)
Trees sorted by Qd ancestry
(b)
No. of Qd alleles
1.4
1.2
1.0
0.8
0.6
chr 1
chr 2
chr 3
chr 4
chr 5
chr 6
chr 7
chr 8
chr 9
chr 10
chr 11
chr 12

Figure 7

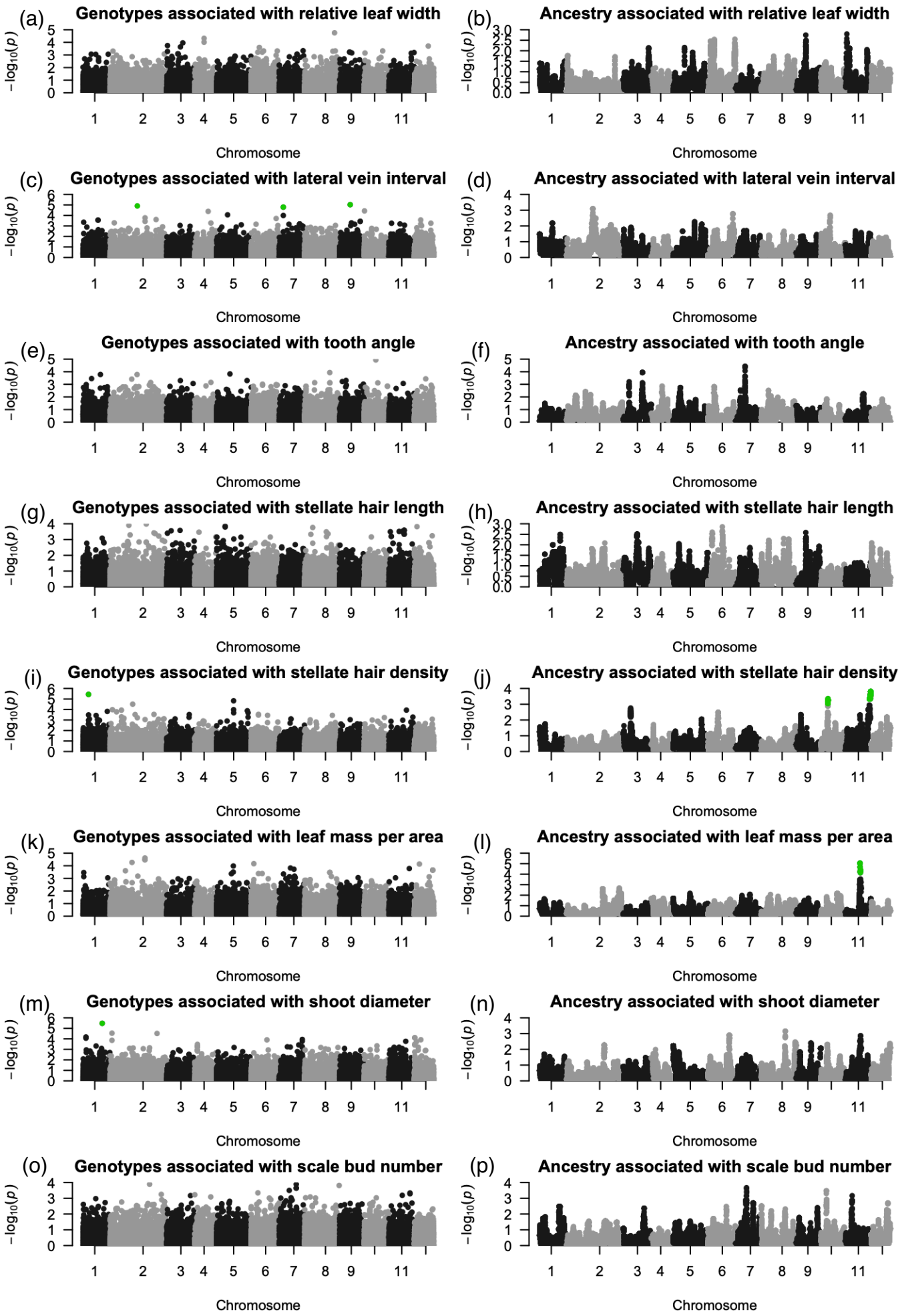
(a)
Genotypes associated with relative leaf width
(b)
Ancestry associated with relative leaf width
(c)
Genotypes associated with lateral vein interval
(d)
Ancestry associated with lateral vein interval
(e)
Genotypes associated with tooth angle
(f)
Ancestry associated with tooth angle
(g)
Genotypes associated with stellate hair length
(h)
Ancestry associated with stellate hair length
(i)
Genotypes associated with stellate hair density
(j)
Ancestry associated with stellate hair density
(k)
Genotypes associated with leaf mass per area
(l)
Ancestry associated with leaf mass per area
(m)
Genotypes associated with shoot diameter
(n)
Ancestry associated with shoot diameter
(o)
Genotypes associated with scale bud number
(p)
Ancestry associated with scale bud number
−log10(p)
Chromosome
1 2 3 4 5 6 7 8 9 11

Table S1. Provenances of sampled trees in inland and coastal sites.

| Provenance | Latitude (°N) | Longitude (°E) | District[1] | Habitat[2] | No. of sampled trees[3] | | | | | | | | | | |
|---|---|---|---|---|---|---|---|---|---|---|---|---|---|---|---|
| | | | | | Inland site | | | | | Coastal site | | | | | |
| | | | | | *Qc* R | *Qc* N | *Qa* | *Qd* R | *Qd* N | *Qc* R | *Qc* N | *Qa* | *Qd* R | *Qd* N | Total |
| Meguma | 45.41 | 141.83 | NN | C | | | 3 | | | | | 8 | | | 11 |
| Bakkai | 45.32 | 141.64 | NWN | C | | | 6 | | | | | 14 | | | 20 |
| Hamayuchi | 45.26 | 141.60 | NWN | C | | | 5 | | | | | | | | 5 |
| Onetomanai | 45.20 | 141.57 | NWN | C | | | 3 | | | | | | | | 3 |
| Toyoushi | 45.10 | 142.43 | NE | C | | | 1 | | 4 | | | | | 7 | 12 |
| Wakasakanai | 45.08 | 141.64 | NWN | C | | | 22 | | 1 | | | 16 | | | 39 |
| Esashi | 44.91 | 142.59 | NE | C | | | | | | | | 10 | | 6 | 16 |
| Teshio | 44.90 | 141.90 | NWS | I | | 1 | | | | | | | | | 1 |
| Saragishi | 44.85 | 141.75 | NWS | C | | | | | 11 | | | | | 23 | 34 |
| Nakagawa | 44.80 | 142.10 | NWS | I | 1 | | | | | | | | | | 1 |
| Omu | 44.60 | 142.80 | O | I | 3 | | | | | | | | | | 3 |
| Bifuka | 44.50 | 142.40 | O | I | 3 | | | | | | | | | | 3 |
| Niupu | 44.50 | 142.60 | O | I | 2 | | | | | | | | | | 2 |
| Okoppe | 44.40 | 143.10 | O | I | 5 | | | | | | | | | | 5 |
| Yubetsu | 44.21 | 143.67 | O | C | | | | | | | | | 2 | 6 | 8 |
| Antaroma | 43.85 | 142.69 | O | I | 2 | | | | | | | | | | 2 |
| Kitami | 43.80 | 143.70 | O | I | 2 | 1 | | | | 4 | 2 | | | | 9 |
| Asahikawa | 43.70 | 142.30 | O | I | 3 | | | | | | | | | | 3 |
| Shintotsukawa | 43.50 | 141.80 | O | I | 1 | | | | | | | | | | 1 |
| Takikawa | 43.50 | 141.90 | O | I | 2 | | | | | | | | | | 2 |
| Bibai | 43.30 | 141.90 | O | I | 1 | | | | | | | | | | 1 |
| Ishikari | 43.20 | 141.30 | O | C | | | | 3 | | | | | 8 | | 11 |
| Mikasa | 43.20 | 141.90 | O | I | 2 | | | | | | | | | | 2 |
| Shihoro | 43.20 | 143.20 | O | I | | | | 6 | | | | | | | 6 |
| Kanayama | 43.10 | 142.40 | O | I | | 1 | | | | | | | | | 1 |
| Shintoku | 43.10 | 142.80 | O | I | 1 | | | | | | | | | | 1 |
| Ikeda | 42.90 | 143.50 | O | I | 2 | | | | | | | | | | 2 |
| Urahoro | 42.80 | 143.70 | O | I | 2 | | | | | | | | | | 2 |
| Orikawa | 42.70 | 140.10 | O | I | | | | | | 3 | | | | | 3 |
| Taiki | 42.50 | 143.40 | O | C | | | | | | | | | 6 | | 6 |
| Donan | 42.20 | 140.10 | O | I | 5 | | | | | 3 | | | | | 8 |
| Ohnuma | 42.00 | 140.60 | O | I | | 1 | | | | | | | | | 1 |
| | | | | Total | 37 | 4 | 40 | 9 | 16 | 10 | 2 | 48 | 16 | 42 | 224 |

[1]Northern provenances in southwestern (NWS), northwestern (NWN), northern (NN), eastern (NE) districts of the northernmost area of Hokkaido and provenances in the other areas of Hokkaido (O)

[2]Inland habitats (I) and coastal habitats (C)

[3]Trees with pubescent shoots are identified to *Quercus dentata* (*Qd*), trees with glabrous shoots in inland habitats are identified to *Q. mongolica* var. *crispula* (*Qc*), and trees with glabrous shoots in coastal habitats are identified to *Q.* × *angustilepidota* (*Qa*).

[3]R: reference samples, N: non-reference samples

(a)

(b)

Figure S1. Photographs of inland site (a) and coastal site (b) in 2017.

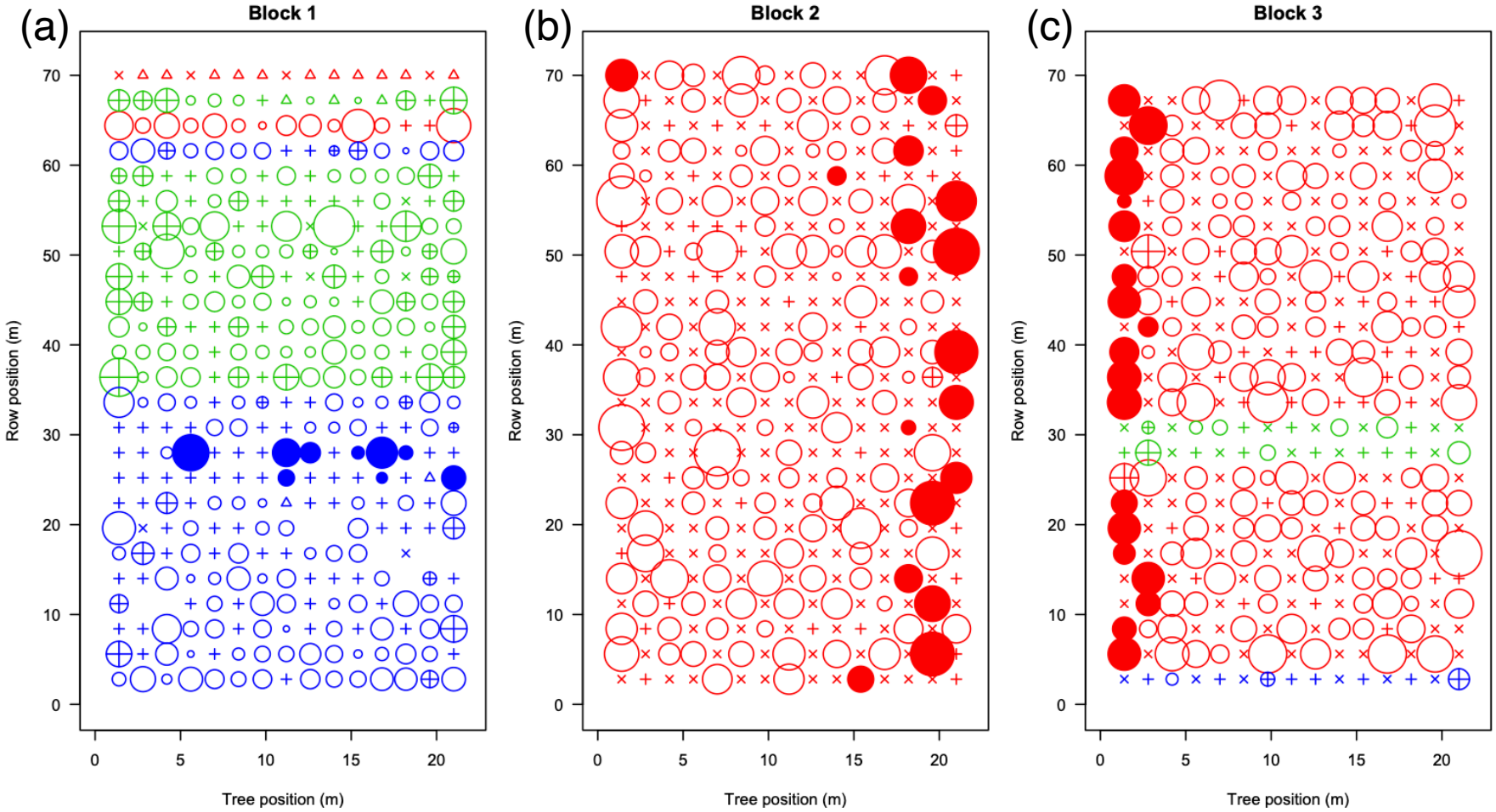


Figure S2. Locations and sizes of trees planted in three blocks (a–c) in inland site. Solid circles, circles with crosses, and open circles indicate sampled reference, sampled non-reference, and non-sampled living trees, respectively. Crosses, + and ×, indicate dead and thinned trees, respectively. Triangles indicate non-experimental trees. Colors indicate taxa: Quercus mongolica var. crispula (red), Q. × angustilepidota (green), and Q. dentata (blue).

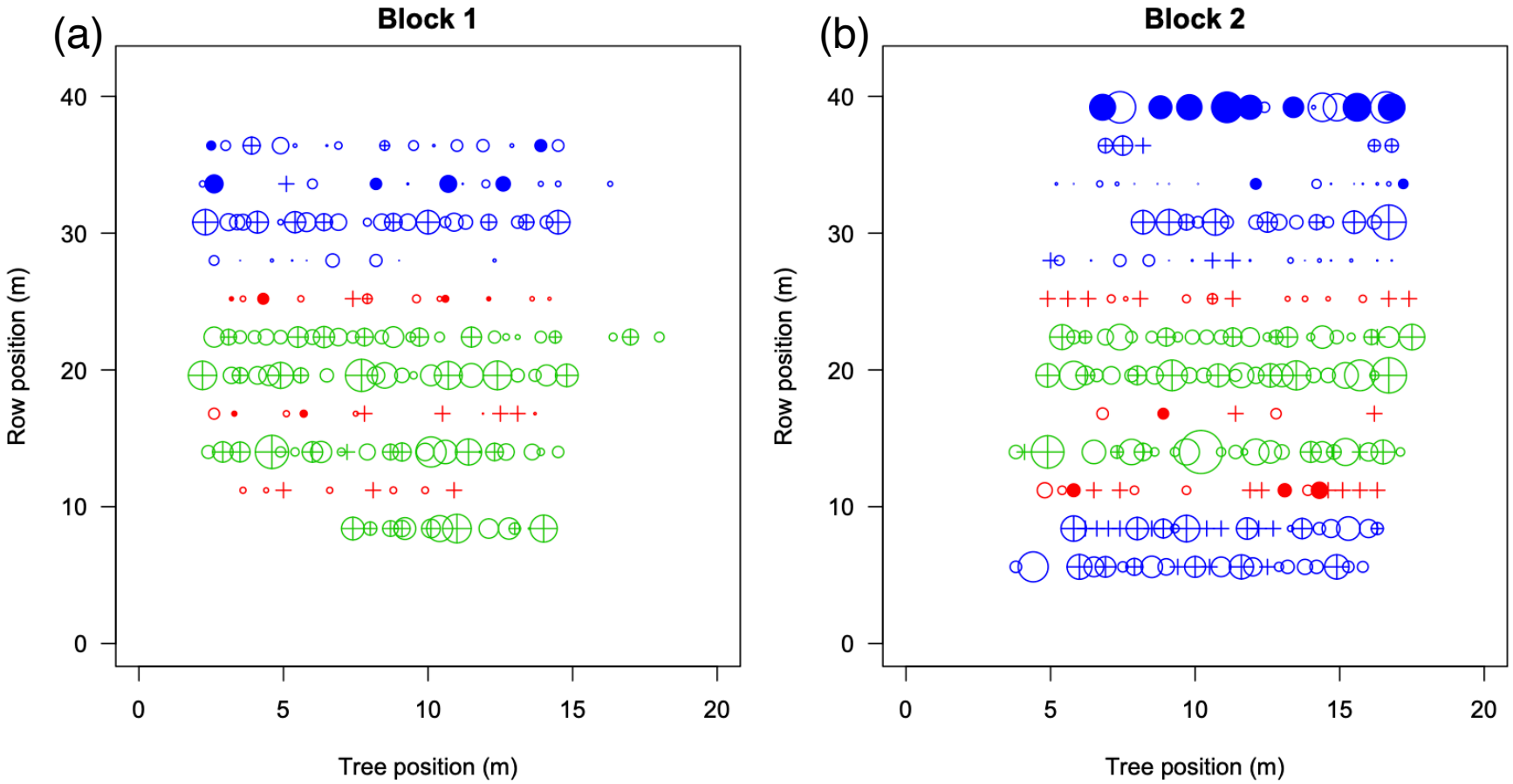


Figure S3. Locations and sizes of trees planted in two blocks (a, b) in coastal site. Solid circles, circles with crosses, and open circles indicate sampled reference, sampled non-reference, and non-sampled living trees, respectively. Crosses, + and ×, indicate dead and thinned trees, respectively. Triangles indicate non-experimental trees. Colors indicate taxa: Quercus mongolica var. crispula (red), Q. × angustilepidota (green), and Q. dentata (blue).

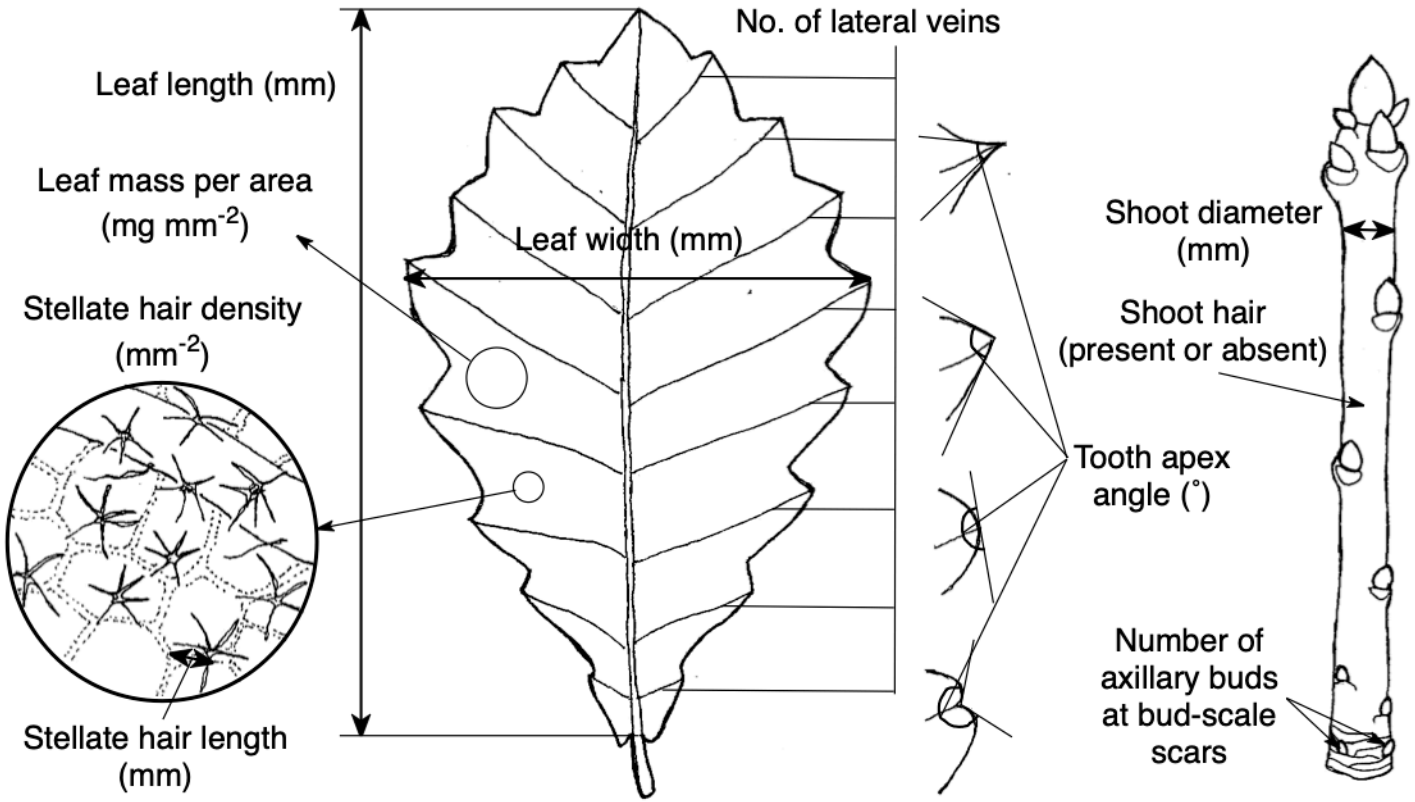


Figure S4. Measurements for morphological traits of leaves and shoots.

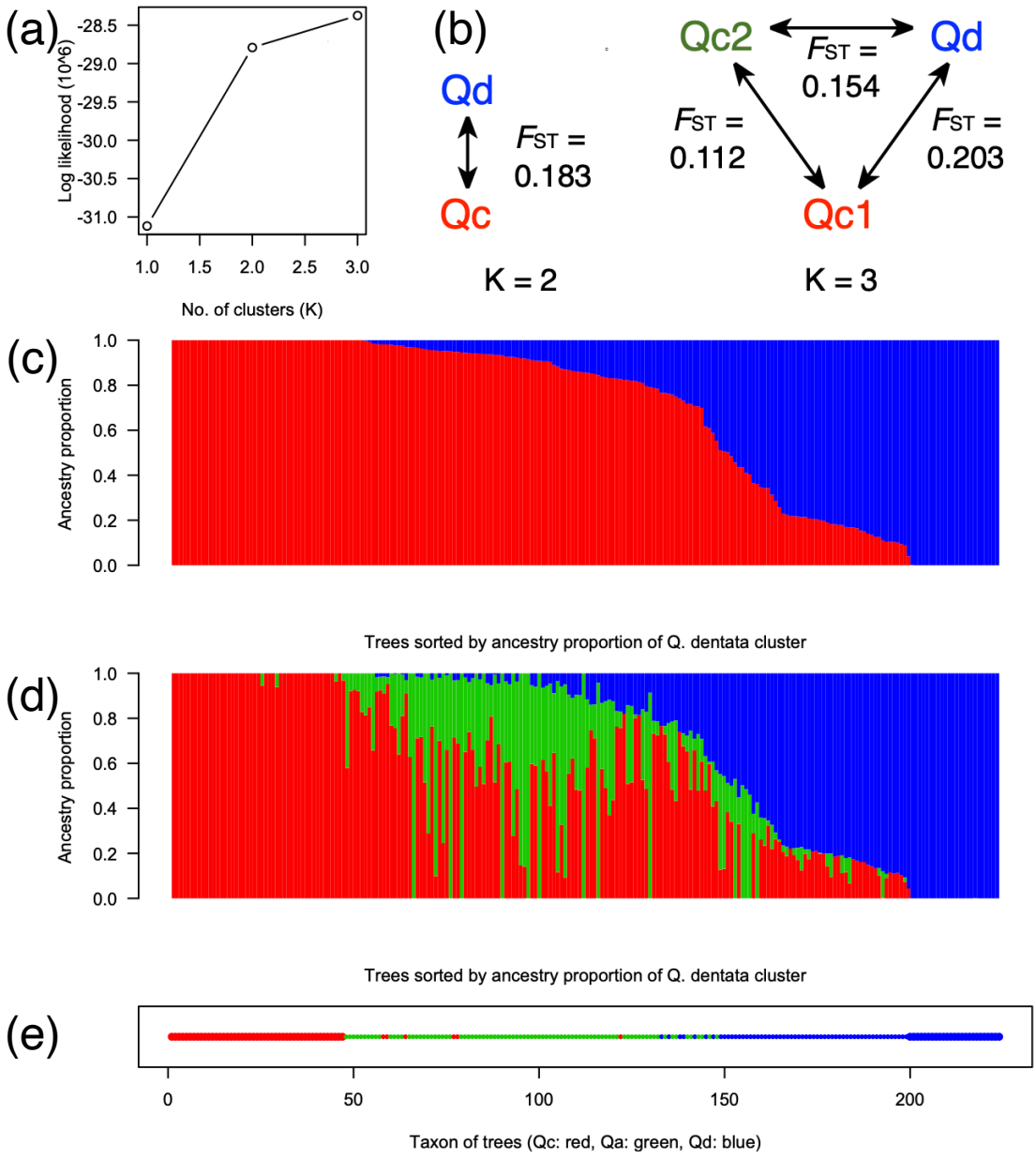


Figure S5. Bayesian clustering of SNP genotypes at ddRAD loci of sampled trees in both inland and coastal sites. Log likelihood when the number of clusters (K) are 1, 2, and 3 (a). Genetic differentiation (FST) between clusters when K = 2 and K = 3 (b). Bar plots of ancestry proportions of trees sorted by the ancestry proportion of clusters, when K = 2 (c) and K = 3 (d). Colors correspond to clusters (b, c, d). Colors of circles indicate taxa: Quercus mongolica var. crispula (red), Q. × angustilepidota (green), and Q. dentata (blue), and enlarged symbols indicate reference samples (e).

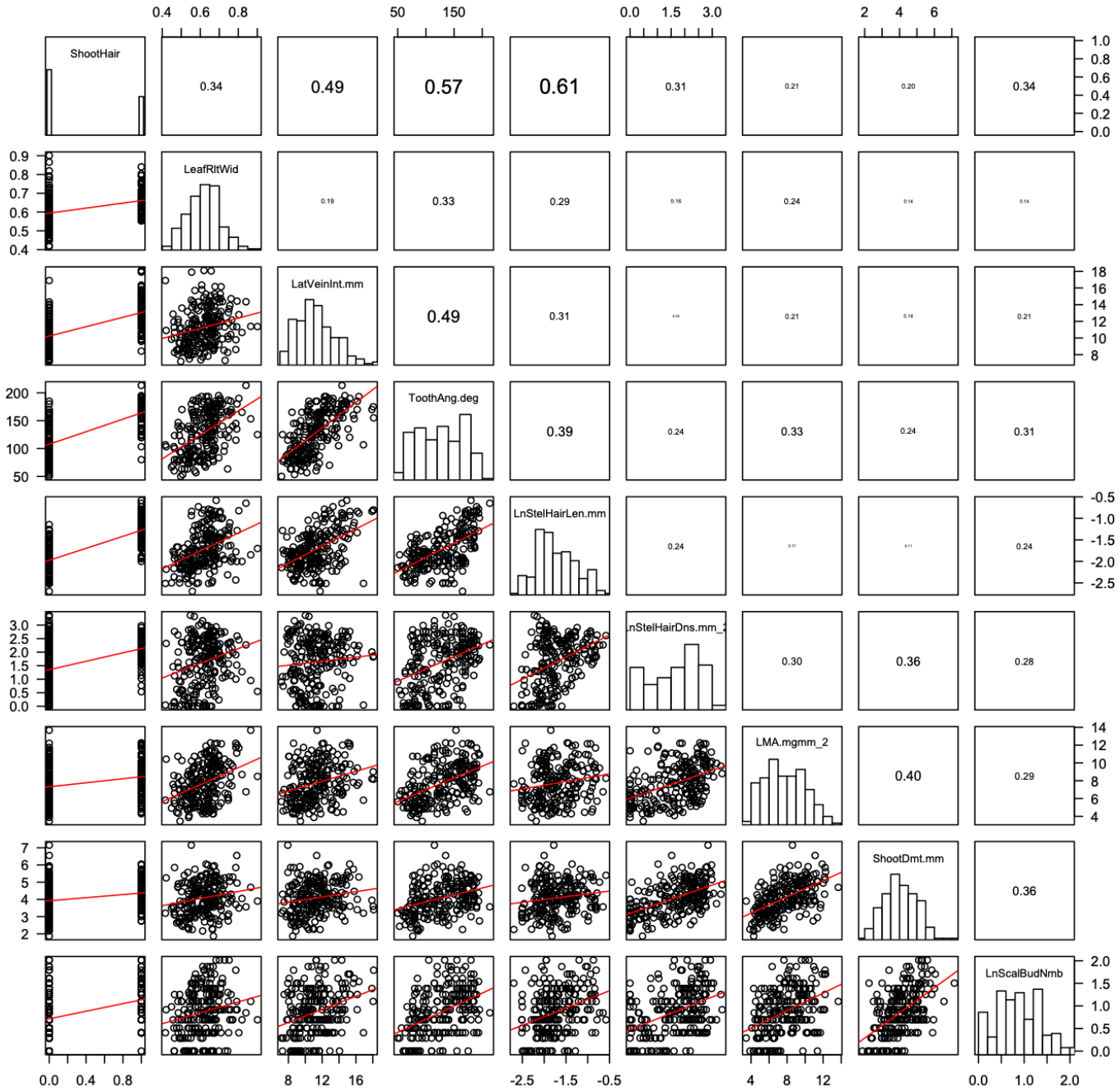


Figure S6. Frequency distributions (scatter plots) and correlations (histograms) for pairs of a taxon-diagnostic trait: shoot hair (0: absent and 1: present) and eight morphological traits: relative leaf width, lateral vein interval (mm), tooth angle (˚), loge length (mm) and loge density (mm–2) of stellate hair on lower leaf surface, lead mass per area (mg mm–2), shoot diameter (mm), and loge number of axillary buds at bud-scale scars. Numbers indicate Kendall's correlation coefficients, and red lines indicate linear regression lines.

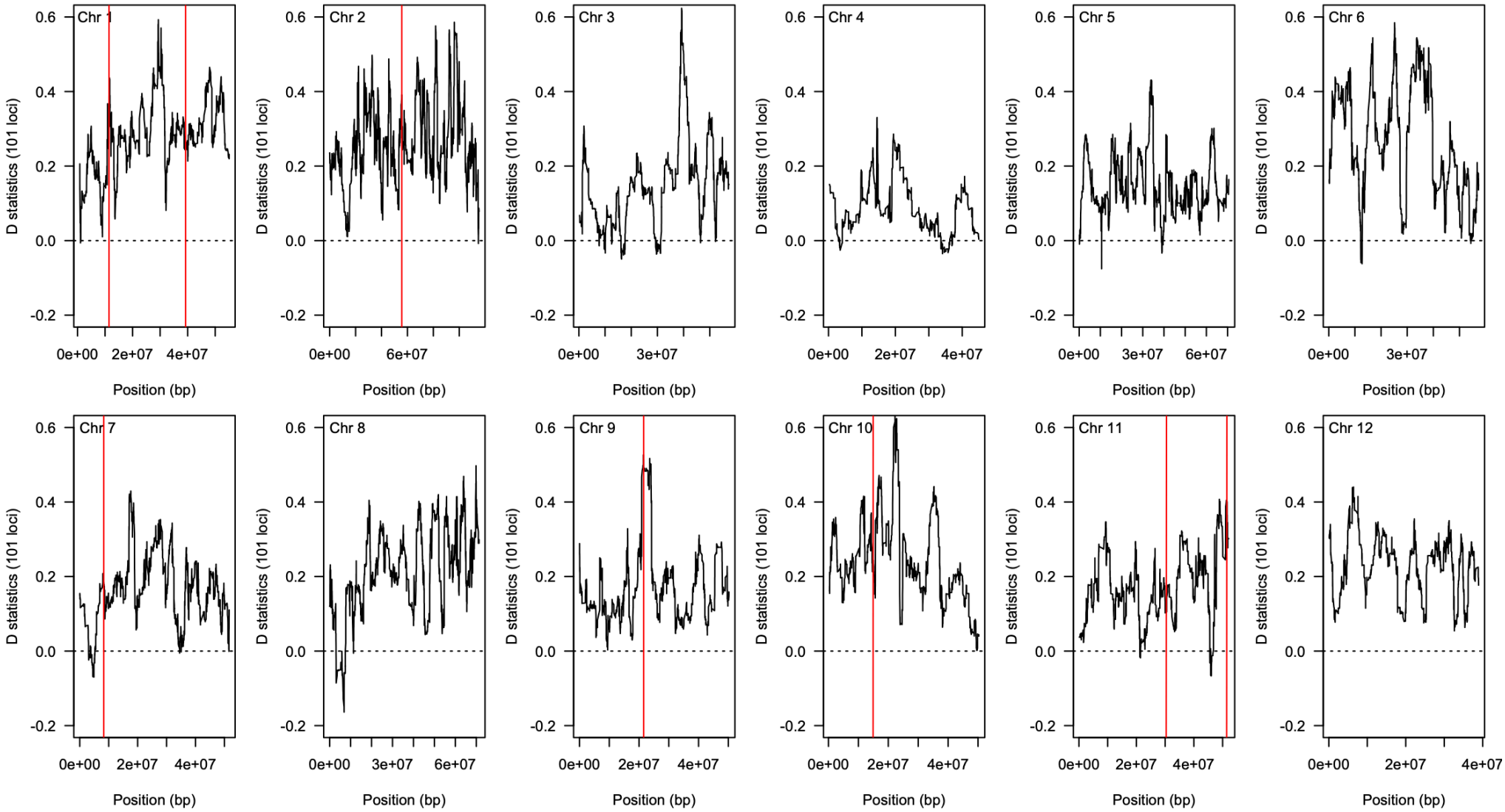


Figure S7. Patterson's D statistics at neighboring 101 ddRAD loci along chromosomes. Positive D values indicate introgression from Quercus dentata to Q. mongolica var. crispula. Red vertical lines indicate positions of trait-associated loci shown in Figure 7 and Table S2.

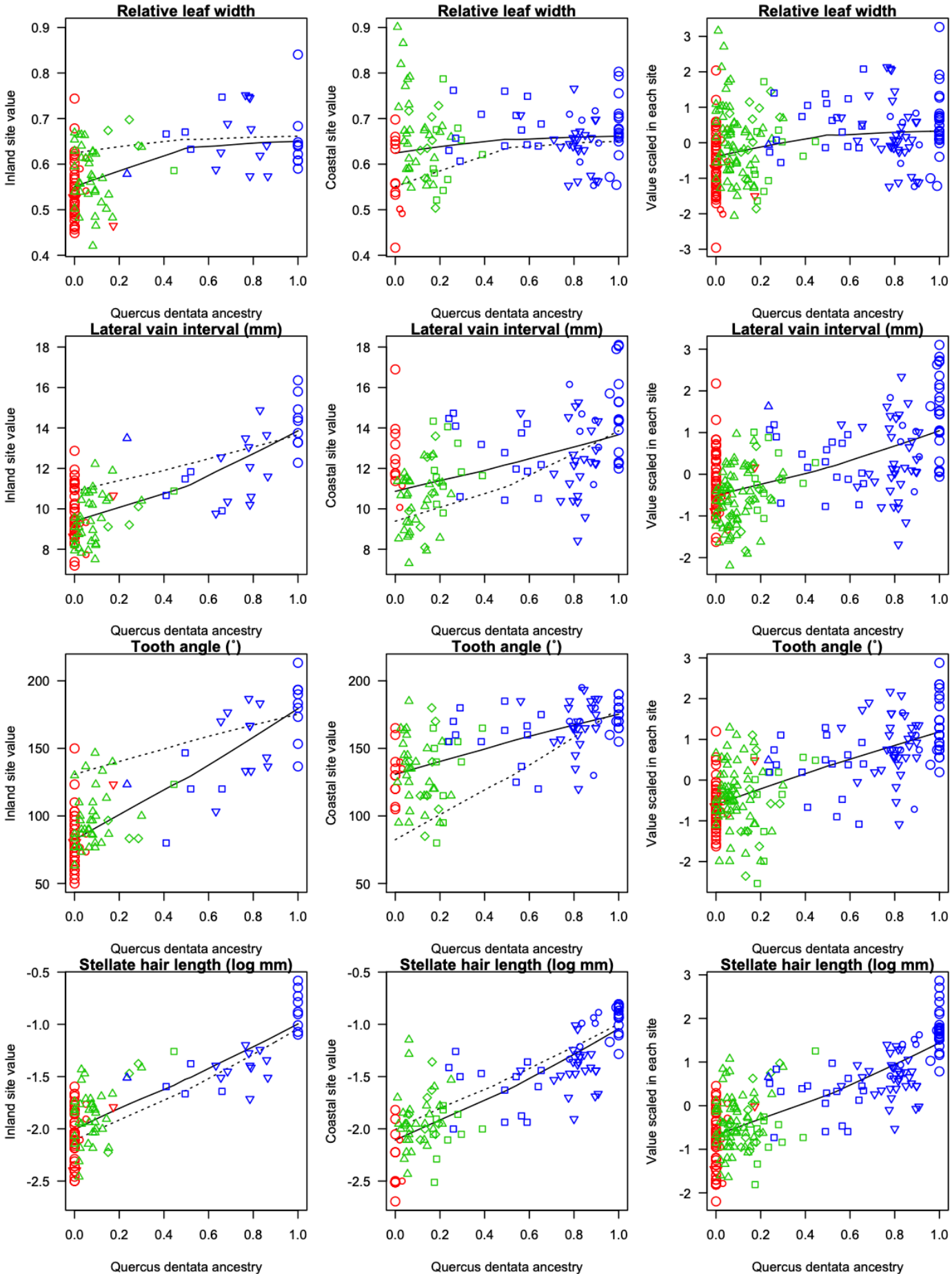


Figure S8. Phenotypic values of four taxon-specific traits in inland (left) and coastal (middle) sites and those values scaled in each site and pooled together (right) in relation to Quercus dentata ancestry. Solid and dotted lines are fitted to observations in the focal site and the other site, respectively, using the lowess method. Symbols are shown in the same way as Figure 1.

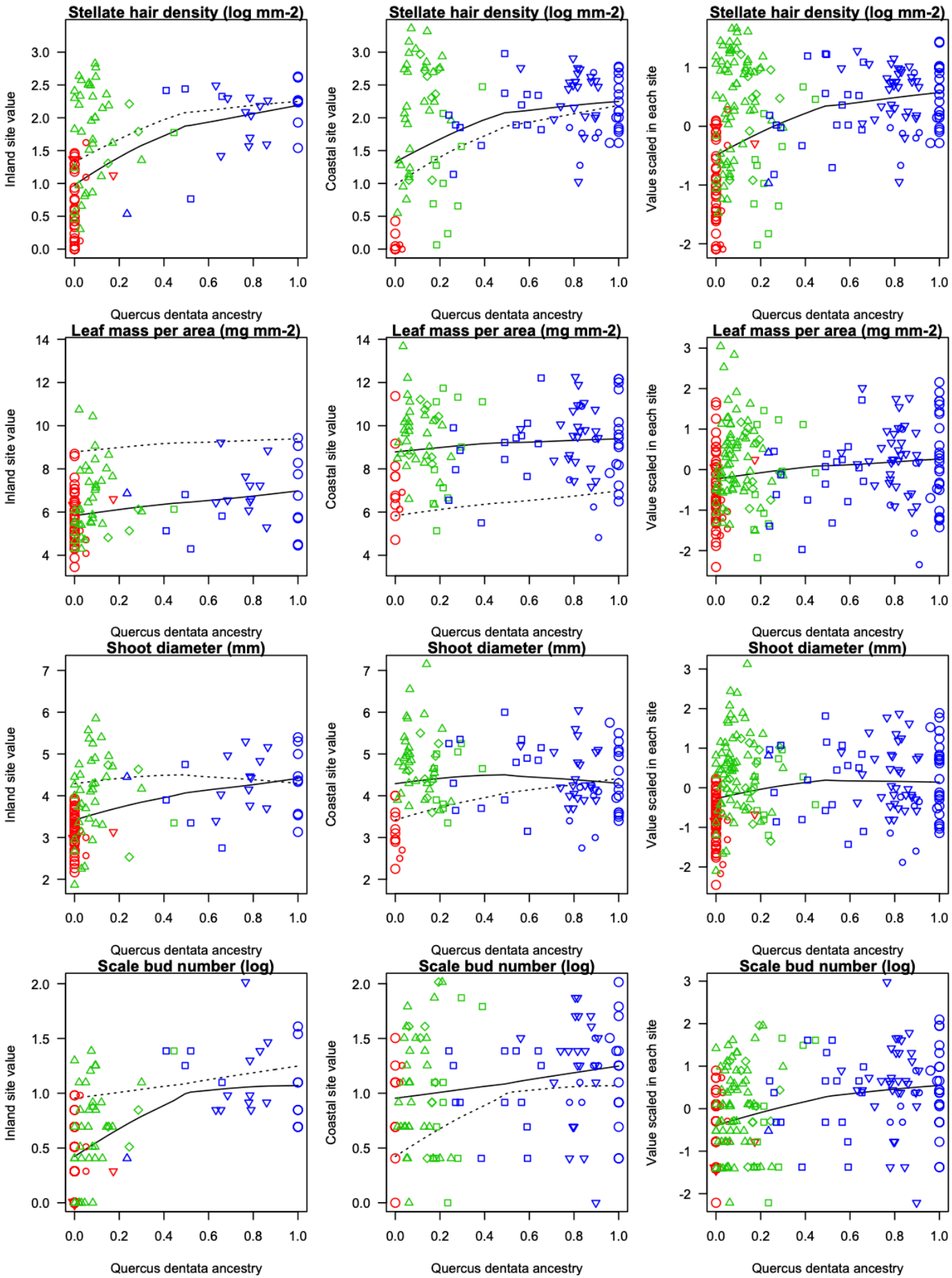


Figure S9. Phenotypic values of four habitat-specific traits in inland (left) and coastal (middle) sites and those values scaled in each site and pooled together (right) in relation to Quercus dentata ancestry. Solid and dotted lines are fitted to observations in the focal site and the other site, respectively, using the lowess method. Symbols are shown in the same way as Figure 1.

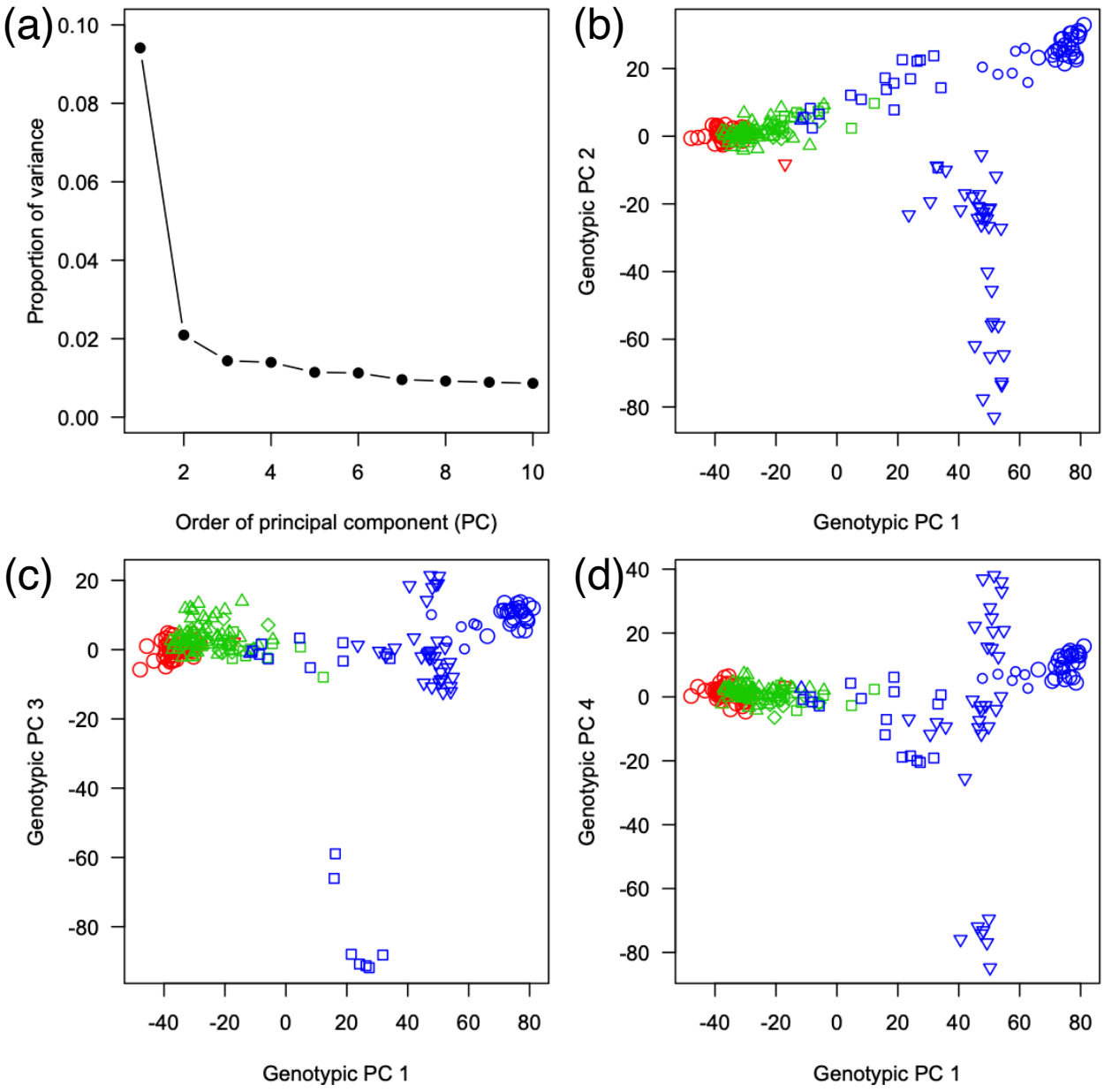


Figure S10. Principal component analysis for SNP genotypes at ddRAD loci of sampled trees in both inland and coastal sites. Proportion (%) of variances for the first 10 principal components (PCs) are shown (a). Coordination of sampled trees on the first and second PCs (b), the first and third PCs (c), and the first and fourth PCs (d) are shown. Symbols are shown in the same way as Figure 1.

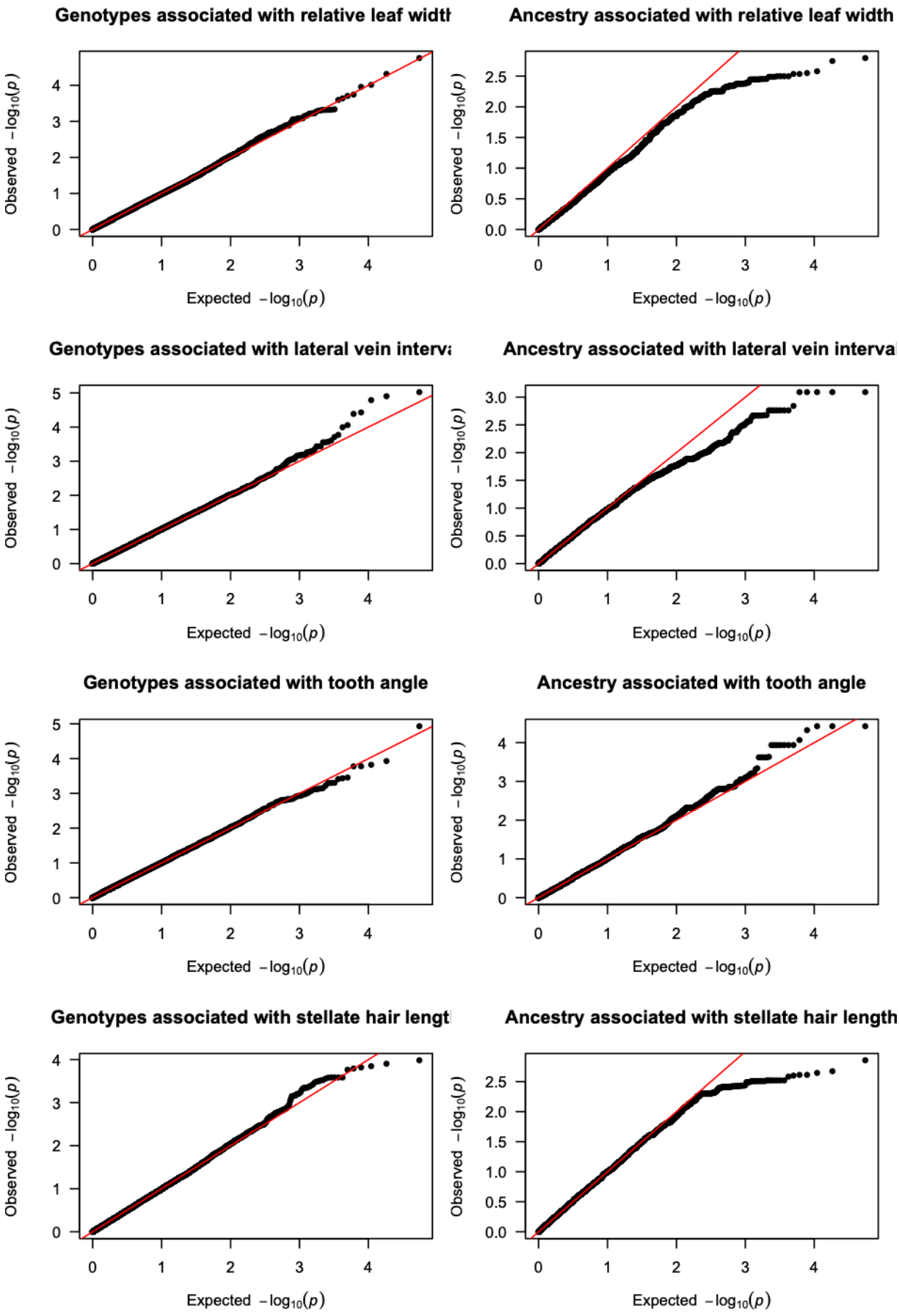


Figure S11. Q-Q plots of expected and observed –log10 p values for four taxon-specific traits. Red lines indicate identical expected and observed –log10 p values.

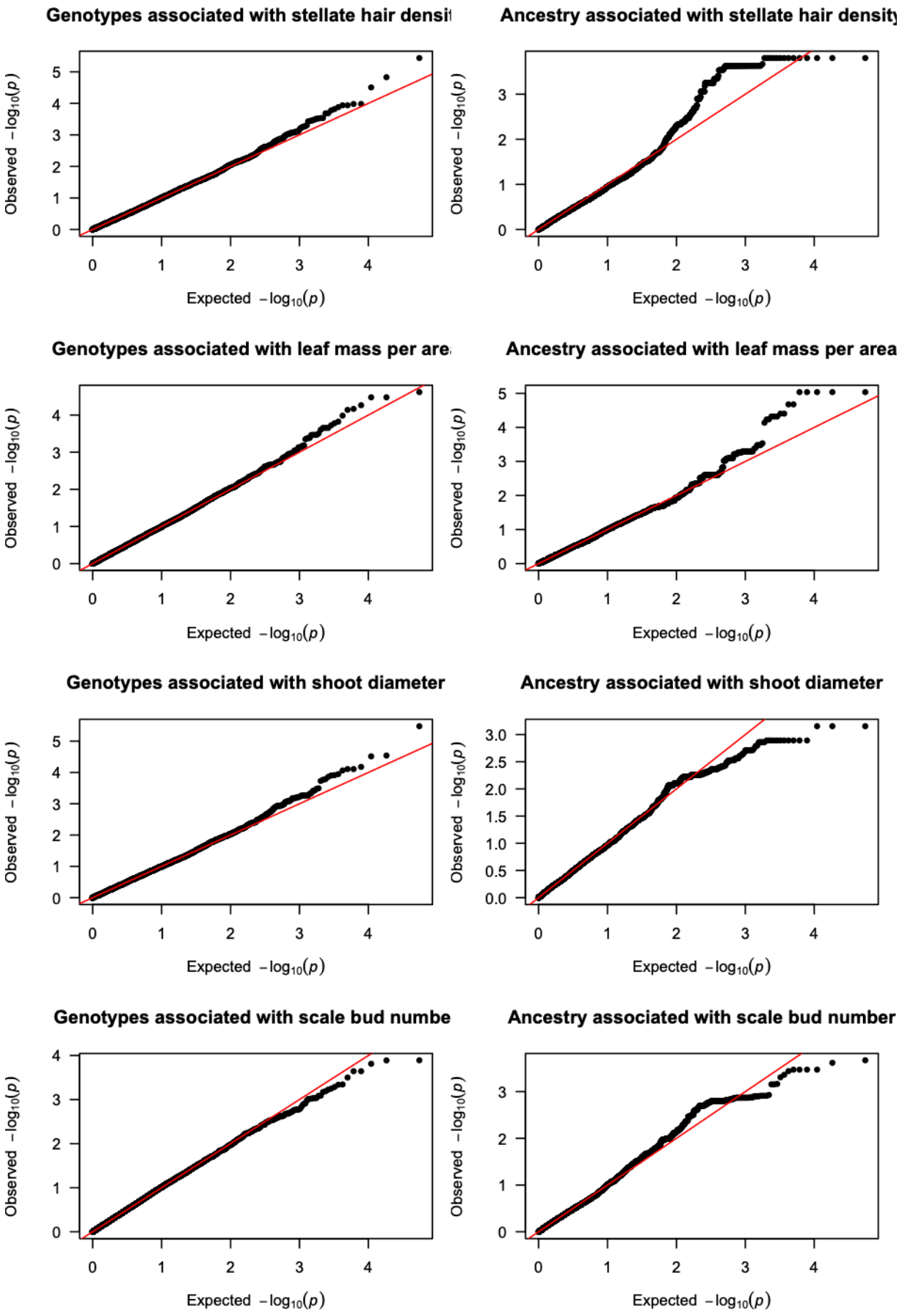


Figure S12. Q-Q plots of expected and observed –log10 p values for four habitat-specific traits. Red lines indicate identical expected and observed –log10 p values.

Table S2. ddRAD loci of SNP genotypes (G) and local ancestry (A) associated with traits (FDR < 0.15) and proteins nearest to or between trait-associated loci obtained from PM1N v2.3 Quercus robur annotation database.

| Chromo- | Position (bp) | | | Genetic | | | | Position (bp) | | | |
|---|---|---|---|---|---|---|---|---|---|---|---|
| some | Start | End | Trait | data | $-\log_{10}p$ | FDR | Protein ID | Start | End | GO term | Protein name [EC] reference |
| 1 | 11432817 | 11432817 | Stellate hair density | G | 5.44 | 0.100 | Qrob_P0619080.2 | 11451267 | 11456090 | 5524 ATP binding, 3678 DNA helicase activity, 43141 ATP-dependent 5'-3' DNA helicase activity | OTU domain-containing protein 5 [EC:3.1.2.15] |
| 1 | 39247601 | 39247601 | Shoot diameter | G | 5.48 | 0.091 | Qrob_P0559890.2 | 39249048 | 39249986 | 3677 DNA binding | |
| 2 | 55663257 | 55663257 | Lateral vein interval | G | 4.90 | 0.148 | Qrob_P0202950.2 | 55665275 | 55671305 | 8152 metabolic process, 16491 oxidoreductase activity | |
| 7 | 8293934 | 8293934 | Lateral vein interval | G | 4.79 | 0.148 | Qrob_P0218810.2 | 8292719 | 8297719 | 16491 oxidoreductase activity, 55114 oxidation-reduction process | 2-hydroxyglutarate dehydrogenase [EC:1.1.99.2] Engqvist et al. (2011) https://doi.org/10.1074/jbc.M110.194175 |
| 9 | 21549823 | 21549823 | Lateral vein interval | G | 5.02 | 0.148 | Qrob_P0026840.2 | 21547671 | 21559909 | 5515 protein binding, 8270 zinc ion binding | |
| 10 | 14717056 | 14754019 | Stellate hair density | A | 3.35 | 0.146 | Qrob_P0142700.2 | 14746075 | 14746713 | 5509 calcium ion binding | |
| 10 | 14926293 | 15132475 | Stellate hair density | A | 3.25 | 0.146 | Qrob_P0555320.2 | 14929357 | 14930715 | 6355 regulation of transcription, DNA-templated, 3677 DNA binding | |
| 10 | 14926293 | 15132475 | Stellate hair density | A | 3.25 | 0.146 | Qrob_P0555330.2 | 14962180 | 14966852 | 3677 DNA binding | |
| 10 | 14926293 | 15132475 | Stellate hair density | A | 3.25 | 0.146 | Qrob_P0555340.2 | 14980666 | 14983249 | 3677 DNA binding | |
| 10 | 14926293 | 15132475 | Stellate hair density | A | 3.25 | 0.146 | Qrob_P0555360.2 | 15020596 | 15022009 | 16853 isomerase activity | Peptidyl-prolyl cis-trans isomerase NIMA-interacting 4 [EC:5.2.1.8] Mokyakova et al. (2014) https://doi.org/10.1134/S1022795414020100 |
| 10 | 14926293 | 15132475 | Stellate hair density | A | 3.25 | 0.146 | Qrob_P0555400.2 | 15050562 | 15054572 | 8152 metabolic process, 3824 catalytic activity, 5975 carbohydrate metabolic process, 16857 racemase and epimerase activity, acting on carbohydrates and derivatives | Ribulose-phosphate 3-epimerase [EC:5.1.3.1] |
| 10 | 14926293 | 15132475 | Stellate hair density | A | 3.25 | 0.146 | Qrob_P0555430.2 | 15096706 | 15098385 | 5515 protein binding | |
| 10 | 14926293 | 15132475 | Stellate hair density | A | 3.25 | 0.146 | Qrob_P0555450.2 | 15111177 | 15114808 | 3676 nucleic acid binding | |
| 10 | 14926293 | 15132475 | Stellate hair density | A | 3.25 | 0.146 | Qrob_P0555460.2 | 15120648 | 15124265 | 3676 nucleic acid binding, 4527 exonuclease activity | |
| 11 | 29866211 | 30015191 | Leaf mass per area | A | 5.04 | 0.051 | Qrob_P0171070.2 | 29865528 | 29873614 | 16020 membrane | |
| 11 | 30838908 | 30926957 | Leaf mass per area | A | 4.40 | 0.110 | Qrob_P0170630.2 | 30885776 | 30889097 | 3824 catalytic activity, 5975 carbohydrate metabolic process, 5509 calcium ion binding, 43169 cation binding, 4556 alpha-amylase activity | Alpha-amylase [EC:3.2.1.1] |
| 11 | 30838908 | 30926957 | Leaf mass per area | A | 4.40 | 0.110 | Qrob_P0170620.2 | 30892546 | 30902560 | 16021 integral component of membrane, 5783 endoplasmic reticulum | Acyl-CoA-dependent ceramide synthase [EC:2.3.1.24] |
| 11 | 30838908 | 30926957 | Leaf mass per area | A | 4.40 | 0.110 | Qrob_P0170610.2 | 30925800 | 30928502 | 5506 iron ion binding, 16705 oxidoreductase activity, acting on paired donors, with incorporation or reduction of molecular oxygen, 20037 heme binding, 55114 oxidation-reduction process | (+)-Abscisic acid 8'-hydroxylase [EC:1.14.13.93] Kushiro et al. (2004) https://www.embopress.org/doi/full/10.1038/sj.emboj.7600121 |
| 11 | 51043879 | 51318001 | Stellate hair density | A | 3.34 | 0.146 | Qrob_P0251550.2 | 51042013 | 51044917 | 3824 catalytic activity, 4722 protein serine/threonine phosphatase activity, 6470 protein dephosphorylation, 43169 cation binding | Protein phosphatase 2C homolog 2/3 [EC:3.1.3.16] Lorenzo et al. (2002) https://doi.org/10.1034/j.1399-3054.2002.1140318.x |
| 11 | 51043879 | 51318001 | Stellate hair density | A | 3.34 | 0.146 | Qrob_P0251510.2 | 51065798 | 51066091 | 5524 ATP binding | Homoserine kinase [EC:2.7.1.39] van Damme et al. (2009) https://doi.org/10.1105/tpc.109.066811 |
| 11 | 51043879 | 51318001 | Stellate hair density | A | 3.34 | 0.146 | Qrob_P0251500.2 | 51079451 | 51086871 | 16020 membrane, 55085 transmembrane transport, 16021integral component of membrane, 22857 transmembrane transporter activity, 22891 substrate-specific transmembrane transporter activity, 5215 transporter activity | |
| 11 | 51043879 | 51318001 | Stellate hair density | A | 3.34 | 0.146 | Qrob_P0251490.2 | 51094139 | 51094775 | 5515 protein binding | |
| 11 | 51043879 | 51318001 | Stellate hair density | A | 3.34 | 0.146 | Qrob_P0251430.2 | 51170728 | 51174833 | 5515 protein binding | |
| 11 | 51043879 | 51318001 | Stellate hair density | A | 3.34 | 0.146 | Qrob_P0251410.2 | 51224590 | 51227672 | 5524 ATP binding, 5634 nucleus, 3682 chromatin binding, 6270 DNA replication initiation, 3678 DNA helicase activity, 42555 MCM complex, 3688 DNA replication origin binding | |
| 11 | 51043879 | 51318001 | Stellate hair density | A | 3.34 | 0.146 | Qrob_P0251330.2 | 51315446 | 51319182 | 5515 protein binding | |
| 11 | 51524292 | 51549907 | Stellate hair density | A | 3.80 | 0.120 | Qrob_P0099790.2 | 51526994 | 51528343 | 8152 metabolic process, 3824 catalytic activity | Isopenicillin-N epimerase [EC:5.1.1.17] |
| 11 | 51524292 | 51549907 | Stellate hair density | A | 3.80 | 0.120 | Qrob_P0099750.2 | 51547955 | 51550308 | 5488 binding | |
| 11 | 51549912 | 51811638 | Stellate hair density | A | 3.63 | 0.120 | Qrob_P0099690.2 | 51599131 | 51604962 | 3677 DNA binding | |
| 11 | 51549912 | 51811638 | Stellate hair density | A | 3.63 | 0.120 | Qrob_P0099650.2 | 51626315 | 51627609 | 6355 regulation of transcription, DNA-templated | |
| 11 | 51549912 | 51811638 | Stellate hair density | A | 3.63 | 0.120 | Qrob_P0099630.2 | 51663338 | 51665116 | 3677 DNA binding | |
| 11 | 51549912 | 51811638 | Stellate hair density | A | 3.63 | 0.120 | Qrob_P0099550.2 | 51716545 | 51717543 | 6355 regulation of transcription, DNA-templated, 3690 double-stranded DNA binding, 5739 mitochondrion | |